Manuscript of the paper entitled 'Late and post-collisional tectonic evolution of the Adria-Europe suture in the Vardar Zone' published in Journal of Geodynamics 149 (2022).
Citation:
Márton, E., Toljić, M., Cvetkov, V. 2022: Late and post-collisional tectonic evolution of the Adria-Europe suture in the Vardar Zone. Journal of Geodynamics 149, 101880.
https://doi.org/10.1016/j.jog.2021.101880

Late and post-collisional tectonic evolution of the Adria-Europe suture in the Vardar Zone

Emő Márton [1 *], Marinko Toljić [2], Vesna Cvetkov [2]

[1] Mining and Geological Survey of Hungary, Paleomagnetic Laboratory, Columbus utca 17-23, H 1145 Budapest, Hungary, paleo@mbfsz.gov.hu
[2] University of Belgrade-Faculty of Mining and Geology, Djušina 7, 11000 Belgrade, Serbia, marinko.toljic@rgf.bg.ac.rs, vesna.cvetkov@rgf.bg.ac.rs,

* corresponding author, e-mail address: paleo@mbfsz.gov.hu

Highlights

- The Western-Central-Eastern Vardar Zones rotated ≈30° CW between 23-18 Ma

- It was connected to extension due to the roll-back of the Carpathian lithosphere

- Earlier compression generated thusting and strike slip faults

- The pile of thrusted segments of the Zone were emplaced onto CCW rotating Adria

- Relevant paleomagnetic results may be interpreted in the light of the above processes

Abstract

The Vardar Zone is a product of the Triassic-Jurassic opening of the Neotethys, Jurassic obduction, Late Cretaceous/Paleogene consumption of the oceanic crust and continental collision. During the last process, the Eastern Vardar Zone was thrust over the Central and eventually both onto the Western Vardar Zone. The present paleomagnetic and structural study provided new results from the first two zones in the Belgrade area. The younger set of data, together with published ones from the third zone, provide firm evidence for about 30° clockwise vertical axial rotation of the Vardar Zone between 23-18 Ma, connected to extension driven by the roll-back of the Carpathians lithosphere.

Earlier, the Vardar Zone was affected by intensive compression generating a nappe pile, comprising the Eastern, Central and Western Vardar Zones. This assembly was eventually thrusted over CCW rotating Adriatic elements in the Paleogene. The rotation triggered a system of right lateral strike slip faults between different tectonic slices in the Vardar Zone. This tectonic model offers a plausible explanation for the paleomagnetic directions of post-folding age of the Upper Cretaceous flysch of the Central Vardar Zone. Nevertheless, the possibility of remagnetization of the magnetite bearing flysch during Late Neogene uplift can not be excluded.

Keywords: Adria–Europe suture, Vardar Zone, paleomagnetism, thrusting, vertical axis rotation

1. Introduction

The Dinarides orogen was created by a Late Mesozoic closure of the northern branch of the Neotethys Ocean, causing a Paleogene continental collision. The Triassic and Jurassic opening of the oceanic domain was followed by Late Jurassic simultaneous divergent obduction of the oceanic lithosphere, (a) over European continental units in the east and (b) over Adriatic continental units in the southwest (in present-day coordinates). The remnant of the oceanic crust was subducted during Cretaceous and Paleogene convergence, resulting in a suture (the Sava-Vardar (Pamić, 2002), Sava (Schmid et al., 2008) or Central Vardar Zone (Toljić et al., 2019) between units of Adriatic and European affinities (Dimitrijević, 1997; Pamić, 2002; Schmid et al, 2008). The tectonic assemblage of this suture zone, established during the Cretaceous-Paleogene subduction and continental collision, was additionally complicated by a Late Oligocene-Miocene extension. This resulted in magmatism within the Vardar Zone and the southern periphery of the Pannonian Basin (Cvetković et al., 2013). This extension was attributed to the roll-back of the subducted Carpathian lithosphere (Horváth, 1993; Bada et al., 2007) which also was responsible for the eastward displacement and counterclockwise (CCW) rotations of the Alp/Carpathian/Pannonian mega unit, as well as the clockwise (CW) rotation of the Tisza-Dacia unit, as constrained by paleomagnetic data (e.g. Márton and Márton, 1983; Márton, 1986, Patrascu et al.,

1990; Márton and Fodor, 1995; Panaiotu, 1998; Márton, 2000). This extension was followed by an inversion since Pliocene to recent times (Bada et al., 2007). This present study was designed to resolve some of these complexities.

The long tectonic evolution of the suture zone between Africa and Eurasia led to the development of a very complex tectonic setting of the Vardar Zone, which is why this suture zone has been interpreted in many different, often contradictory, ways (Supplement 1). Pamić (2002) defined the Sava-Vardar Zone as the most internal tectonostratigraphic unit of the Dinarides and Hellenides; Dimitrijević (1997) divided the Vardar Zone into Internal, Central, and External sub-zones; Karamata (2006) distinguished the Main basin of the Vardar Ocean, the Kopaonik block and ridge unit, the Vardar Zone western oceanic basin, and the Jadar block terrain; Schmid et al. (2008) divided the Vardar Zone into three major tectonic units: the Eastern Vardar ophiolitic unit, the Sava suture zone, and the Jadar-Kopaonik unit with obducted Western Vardar ophiolites. In order to avoid unnecessary complications in this paper the terminology by Toljić et al. (2019) will be followed (Fig. 1).

The Eastern Vardar Zone comprises ophiolites, Lower Cretaceous paraflysch (Dimitrijević, 1997) and Upper Cretaceous shallow water clastites and carbonates in the east, passing into more distant clastic/carbonate turbidites in the west (Toljić et al., 2018). The Central Vardar Zone, the suture, is a domain of Upper

Cretaceous flysch. The Western Vardar Zone is built up from Paleozoic basement, Triassic sediments and volcanics. These, with the ophiolitic mélange and obducted ophiolites of the Western Vardar Zone (see Fig. 1) were obducted over the Adria derived Drina-Ivanjica unit, now forming part of the Dinaride Ophiolite Zone (Toljić et al., 2019, Fig. 1). These successions were then overlain by Albian through Maastrichtian sediments.

The first results of modern paleomagnetic investigations relating to the Vardar Zone were from the Fruška Gora Mts (Lesić et al., 2007; Cvetkov et al., 2012) where Oligocene latites and contact metamorphosed flysch sediments indicated significant vertical axis clockwise (CW) rotation during Early Miocene, followed by about 40° vertical axis counterclockwise (CCW) rotation in post-Middle Miocene times.

Recent anisotropy of magnetic susceptibility (AMS) and paleomagnetic investigations (Lesić et al., 2013, 2019) have been made in the wider Kopaonik (plutons and dacitic andesites) and Rudnik (Oligocene-Lower Miocene igneous rocks) areas (Fig. 1). They yielded good paleomagnetic results that suggested a post-Oligocene rotation of about 35° CW around vertical axis, with respect to the present north.

The area south of Belgrade has special tectonic interest being the locus of the final closure of the Vardar ocean where rocks belonging to the Central Vardar

(suture) Zone and those related to the Eastern Vardar Zone, are accessible for structural observations and paleomagnetic sampling. In order to increase the understanding of the tectonic history of the complicated Vardar Zone of Serbia we carried out here paleomagnetic and structural study, intending to interpret the results in the context of previously obtained data from Western Vardar Zone.

2. Geological background of the Belgrade area

Around Belgrade, Mesozoic ophiolites, Cretaceous sediments and Oligocene igneous rocks outcrop below the Neogene sediments of the Pannonian Basin (Fig. 2). The Mesozoic lithostratigraphy forms two paleogeographic domains, separated by the Bela Reka Fault (Toljić et al., 2018), which is a complex NNW-SSE oriented fault system representing the basal thrust of the Eastern Vardar Zone over the flysch of the Central Vardar (suture) Zone (Fig. 2).

East of the Bela Reka Fault there are serpentinized peridotites, ophiolitic mélange, Jurassic radiolarites and marls, associated with syn-depositional basalts. The tectonized ophiolitic mélange contains radiolarite fragments of Lower Ladinian to Lower Tithonian age (Bragin et al., 2011). A distinctive lithostratigraphic feature of the Eastern Vardar Zone is the Lower Cretaceous paraflysch, covering ophiolites

and an ophiolitic mélange, that was tectonically emplaced at the active European margin (Dimitrijević, 1997; Schmid et al., 2008). The Beriassian-Valanginian paraflysch sequences show weak turbidite features and comprise laminated claystones, siltstones, marls, marly limestones, calcrudites and calcarenites. The paraflysch changes upwards into Valanginian-Barremian marls, claystones, and marly limestones with cephalopods, shallow water clastites and carbonates of the Urgonian facies, followed by Albian sediments of various facies and Albian-Cenomanian continental clastic sediments. Extension during Coniacian-Santonian caused subsidence and the deposition of shallow water carbonates (Toljić et al., 2018), associated with syn-depositional basalts, trachydacites and their volcanoclastics (Toljić et al., 2020). Basalt and locally lamprophyre dykes also intrude Lower Cretaceous sediments. The largest intrusion of lamprophyre (Tešića quarry) has been dated as 86.80 ±0.5 Ma (Sokol et al., 2020). The Late Cretaceous sedimentation terminated with the deposition of limestones, marls, marly limestones, and sandstones of Coniacian-Maastrichtian age (for further details on age of Mesozoic sediments see Toljić et al., 2018 and references therein).

West of the Bela Reka Fault, in the Central Vardar Zone, the oldest sediment cropping out is the Campanian-Maastrichtian flysch (Fig. 2), comprising marls (dominant members), sandy marls, carbonate sandstones and sandstones (Toljić

et al., 2018). During the Early Paleogene molasse was deposited (Anđelković, 1973).

The sediments, east of the Bela Reka Fault, were intruded by lamprophyres (30.88 Ma, Cvetković et al., 2004), a shallow subsurface granodiorite body and numerous dykes of latites, quartz-latites, dacites, rhyolites (25.12–23.27 Ma, Vasković and Matović, 1996). On the western side of the same fault, highly altered dacitic dykes, probably of similar ages, intrude Upper Cretaceous flysch deposits around Babe. Although their exact ages are not known, they cannot genetically originate in the domain of the subduction trench, represented here by the Upper Cretaceous flysch of Central Vardar Zone, but are most likely the results of post-orogenic petrogenesis (Cvetković et al., 2013). The Babe dacites also share the same metallogeny as the Oligocene magmatites from the Belgrade area. All the above points to the Oligocene age of dacite in the Babe region.

3. Paleomagnetic investigation

3.1. Sampling

The sampling localities are distributed between the Eastern Vardar Zone (in the Avala Mts area) and the Central Vardar Zone (Fig. 2). The paleomagnetic samples were drilled with portable gasoline powered drills with water cooling. The cores were oriented magnetically and with a sun compass when required (e.g. sampling along a railway line).

From the Eastern Vardar Zone well-bedded Coniacian-Maastrichtian limestones (localities 6-8, Fig. 2) and Campanian marly limestone (locality 15, Fig. 2) were drilled from the Avala Mts, where a subsurface granodiorite intrusion is known to have heated and even contact metamorphosed Cretaceous sediments. In addition Upper Oligocene dykes of latite or quartz-latite composition (sites 5, 11-13, 19, Fig. 2) were sampled, including contact metamorphosed host rock at site 5 (Table 1).

West of the Bela Reka Fault, Campanian-Maastrichtian marly limestones (localities 3, 14 and 21, Fig. 2) and marls (localities 1, 2, 4, 9, 9a, 14a, 10, 10a, 20,

17, 16, Fig. 2), a Middle Maastrichtian marlstone (locality 18, Fig. 2) and an Upper Maastrichtian fine grained sandstone (locality 22, Fig. 2) were sampled.

All the sampled sediments were well-bedded, mostly monoclinally tilted (see Table 1) and appeared unweathered. The ages of Mesozoic sediments had been determined by earlier research (e.g. Anđelković, 1973) and more recent studies (Toljić et al., 2018 and references therein). The ages of Cenozoic volcanics have been determined from available publications (Vasković and Matović, 1996; Cvetković et al., 2004).

3.2 Laboratory measurements

From the drill cores, standard size specimens were cut in the laboratory. The natural remanent magnetization (NRM) of the specimens was measured using JR-4, JR-5 and JR-5A magnetometers (AGICO, Brno). This was followed by measurements of the anisotropy of magnetic susceptibility (AMS) using KLY-2 and MFK1-A kappabridges (AGICO, Brno). The AMS data were evaluated with computer programs on sample level by Aniso (Bordás, 1990) based on Jelínek (1977) and on site/locality level by ANISOFT 4.2 and 5.1 (Chadima and Jelínek, 2008; Chadima et al., 2018) based on Jelínek (1978, 1981). Next, pilot specimens were demagnetized in several steps from each locality/site either by stepwise

alternating field (AF) demagnetization (LDA-3A, AGICO and AFD300, Magnon, Dassel) or by thermal demagnetization (TSD-1, Schonstedt Instrument Company, Reston and MMTD80, Magnetic Measurements, Aughton). Susceptibility was monitored during thermal demagnetization. According to the behaviour of pilot specimens during demagnetization, the remaining samples from each locality/site were demagnetized with the method which was the most efficient to define the NRM components. The demagnetization curves (Zijderveld, 1967) were analyzed for linear segments (principal component analysis, Kirschvink, 1980). Statistical evaluation on locality/site level was based on Fisher (1953) method.

In order to identify the ferrimagnetic minerals, magnetic mineralogy experiments were carried out on selected specimens. These experiments included temperature vs. susceptibility measurements up to 700°C, either from liquid nitrogen temperature or from room temperature (using KLY-2 combined with CS-1 or CS-3 both from AGICO, Parma et al., 1993; Hrouda, 1994), IRM acquisition experiments (either with a Molspin Pulsmagnetizer or a MMPM10 magnetizer, Magnetic Measurements) and the stepwise thermal demagnetization of the 3-component IRM (Lowrie, 1990), accompanied by susceptibility monitoring.

3.3. Paleomagnetic results

3.3.1 Magnetic mineralogy

In the igneous rocks, the magnetic mineral identified was magnetite (Fig. 3, S53A and S140A), accompanied by a substantial amount of paramagnetic minerals in quartz latite (S53). Upper Cretaceous marls with susceptibilities in the 10^{-4} SI range (Fig. 3, S16, S108), which is the highest among this type of rocks, also reveal that magnetite was only a minor contributor to the low field susceptibility.

Consequently their AMS fabrics were expected to be governed by paramagnetic minerals.

IRM experiments followed by thermal demagnetization of the 3-component IRM carried out for Cretaceous marls and for shallow water carbonates also indicated magnetite as the dominant magnetic mineral (Fig. 4).

3.3.2. Paleomagnetic directions

Paleomagnetic directions characteristic for each locality/site were obtained from the results of stepwise demagnetization and component analysis of the demagnetization curves. Practically single-component NRM characterized the shallow water carbonates as well as the igneous rocks from the Avala area (Fig. 5,

locality 6 and sites 5 and 13). The marls from the Central Vardar Zone exhibited either single (Fig. 5, localities 17 and 4) or composite (Fig. 5, localities 1 and 10a) NRM. In case of composite remanence, the component decaying towards the origin of the Zijderveld diagrams was interpreted as the characteristic remanent magnetization (ChRM). Instability of the NRM was observed only in one case (an Oligocene dyke, site 11).

As a result of principal component analysis and statistical evaluation of the ChRMs, paleomagnetic mean directions with good statistical parameters were defined for most of the sedimentary localities/igneous sites. For localities, 10a and 18 the low-unblocking temperature component was also quite consistent and thus tabulated along with the respective ChRM.

On the eastern side of the Bela Reka Fault (Avala Mts. area, Fig. 2), the site mean paleomagnetic directions for the dykes (Fig. 6A, red arrows) were well-clustered (Fig. 6B and C, red points) and the between-site reversal test is $Rb_{(i)}$ (McFadden and McElhinny, 1990). We interpret these directions as primary. In the same area, the shallow water carbonates (Fig. 6A, black arrows) have magnetizations of post-tilting age and hence were considered to have been remagnetized during the Oligocene magmatic activity (Fig. 6B and C). It is likely that this remagnetization was mainly due to the large subsurface Avala intrusion, and occasionally due to contact metamorphosis related to a dyke (Table 1, site 5). This is not only

suggested by the paleomagnetic directions of the shallow water carbonate sediments, but also by the unusually high susceptibilities (Table 3, localities 6-8) compared to the “normal” Adriatic platform carbonates (e.g. Márton et al., 2008), which can be the consequence of infiltration by magmatic fluids.

The combination of the results from the Oligocene dykes and remagnetized limestones defined an overall mean paleomagnetic direction which suggested some 33° CW vertical axis rotation with respect to the present north, after the Oligocene (Fig. 6B and Table 2).

On the western side of the Bela Reka Fault, the situation was more complicated. There are two groups of ChRM directions, both of them characterized by negative tilt test (Fig. 6F and I). One of these, comprising the majority of the localities (Fig. 6A, long blue arrows), is of normal polarity, except locality 1, displays a smeared distribution between moderately westerly and moderately easterly declinations before tilt corrections (Fig. 6E). The low temperature unblocking components at localities 18 and 10a (Fig. 6A, hollow blue arrows) belong to this group. The overall-mean declination for this group is close to that of the present north (Fig. 6E).

The ChRMs for localities 18 and 10a from the Central Vardar Zone and also for locality 15 in the vicinity of the Bela Reka Fault, formed a second group, together with an earlier studied limestone locality from the “Rudnik” segment of the

Central Vardar Zone (Fig. 1, and reference to Lesić et al., 2019). They exhibited reversed polarity magnetizations, suggesting about 76° vertical axis CW rotation (Fig. 6 H).

3.3.3. Magnetic Anisotropy

The magnetic fabrics of the dykes from the Avala area were quite weak (K1/K3 is max. 1.032), the shape of the AMS ellipsoid was prolate for sites 11 and 12 and oblate for sites 5, 13 and 19. In contrast, the sediments of the Central Vardar (suture) Zone were characterized by fairly high K1/K3, reaching the value of 1.12. (Table 3). Bedding parallel and dominant AMS foliations (Table 3) suggested weak deformation. Nevertheless, the magnetic lineations were mostly well defined on locality level (error angle between maximum and intermediate axes of the AMS ellipsoid is smaller than 15°, see Table 3). Exceptions are shown as hollow arrows in Fig. 7.

Anisotropy of the remanent magnetization (AARM) was measured for selected specimens. Comparison between the AMS and AARM fabrics for the same locality reveal that the maxima in both cases are practically N-S oriented (Fig. 7D and E).

4. Deformation history

4.1. Methods of the structural analysis

In order to understand the deformational evolution, structural and kinematic field study was carried out in outcrops of the Mesozoic and Neogene sediments and volcanites in the vicinity of Belgrade. Structural analysis included observations, like bedding orientation and its geopetal properties, fold geometries, superposition of fold structures, and relations between folds and faults. For faults, the positions of structures, their kinematic characteristics and potential reactivation were determined, based on indicators such as slickensides, steps, and rare Riedel shears, all providing the directions of the tectonic transport. Temporal relations between the deformations were determined based on the superposition of the structures, relying on the order in which faults of different geometries and kinematics cross-cut each other, on the directions of the intruded dykes, on the cross-cut relations of faults and dykes, on the superposition of fold structures, and on the stratigraphic positions of the rocks which contain the studied structures. The data were analysed from the viewpoint of the general tectonic

evolution as well as the mechanisms of possible rotation of tectonic units and/or individual blocks.

During field observations more than 700 structural data had been collected. These were evaluated and the results were presented in structural diagrams for kinematic and structural data visualization, processing and analysis, TectonicsFP (Ortner et al., 2002) and Open Stereo (Grohmann and Campanha, 2010) were used.

4.2. Results of the structural analysis

Structural analyses suggested that the area underwent poly-phase tectonic evolution, characterized by alternating periods of compression and extension. Taking into account the Late Cretaceous-Oligocene age of the rocks studied magnetically, the main focus was on the effects of the Late Cretaceous and younger deformations.

The fault pattern was dominated by NNW-SSE oriented structures, representing part of a complex thrust defined as the Bela Reka Fault (Fig. 2). The expression of tectonic fabrics, kinematic features, and superposition of faults in the Belgrade area indicated that the Bela Reka Fault was the major structure separating the Upper Cretaceous flysch of the Central Vardar Zone, in footwall, from the Eastern

Vardar Zone hanging wall (Toljić et al., 2018, 2019). The kinematic data indicated that the Bela Reka Fault was associated with WSW vergent thrusts. The reconstructed stress axes showed tectonic transport towards the WSW (Fig. 2 and Fig. 8A). Thrusts were crosscut by co-genetic right-lateral transcurrent NE-SW oriented faults and were also active in a strain field in which the maximum stress axis was oriented ENE-WSW, in present coordinates (Fig. 2 and Fig. 8B).

Near Belgrade, two other groups of faults were analysed. The first was made up of right-lateral transcurrent faults with ENE vergences (Fig. 8C) which were parallel to the Bela Reka Fault. They were crosscut by reverse faults, with almost E-W directions (Fig. 8D), which also intersect the Bela Reka Fault, indicating that they are younger. For these transcurrent and reverse faults, the compression axis was N-S, suggesting that they formed one co-genetic group of structures. Our field data suggested that the Bela Reka Fault was also partly re-activated by dextral transcurrent movement.

Polyphase contractional tectonics were also recognized in the fold structures in the Cretaceous sediments on both sides of the Bela Reka Fault. The field studies, and statistical analyses of bedding plane orientations in Mesozoic sediments, east of the Bela Reka Fault, indicated that WSW vergent folds with axes were oriented predominantly NNW-SSE. Fold structures in the Upper Cretaceous flysch, west of the Bela Reka Fault, showed W and WSW vergences, while statistical fold axes

showed local variations in direction (Fig. 9). Folds south and southeast from Barajevo (Fig. 2) had W vergences and axes oriented N-S (Fig. 9A). Those between Barajevo and Sremčica (Fig. 2) had W and SW vergences and N-S axes, with some subordinate NW-SE axes (Fig. 9B). Flysch in the northern segment of the suture zone, around Ostružnica (Fig. 2), was deformed into folds with SW and W vergences and fold axes in a NW-SE direction, and subordinately N-S (Fig. 9C).

It is important to note that Neogene sediments were only slightly faulted and tilted, and did not show any major fold structures, or signs of earlier active transcurrent faults.

The entire Belgrade area had undergone two phases of extension. The first during the Coniacian-Santonian (Toljić et al., 2018), and the second in Oligocene to Miocene times (Vasković and Matović, 1996; Stojadinović et al., 2013, 2017). The Late Oligocene-Miocene extension reactivated the older faults and normal faults developed, as also observed in Mesozoic sediments and serpentinized peridotites. Some of the normal faults were oriented NNW-SSE (Fig. 8E) and were active in ENE-WSW oriented field of extension (e.g. orogen-perpendicular extension), although the others had ENE-WSW (Fig. 8F) orientation and had undergone a NNW-SSE oriented orogen-parallel extension. Several segments of the normal faults, from both groups, were intruded by dykes of Upper Oligocene magmatites (Fig. 8G).

5. Discussion

5.1. Discussion of the paleomagnetic and magnetic anisotropy results

Earlier published paleomagnetic results from the Rudnik-Kopaonik block (Fig. 1B) had defined about 30-35° post-Oligocene vertical axis CW rotation, with respect to the present north, that had affected the Jadar-Kopaonik Unit, together with obducted Western Vardar ophiolites (Lesić et al., 2019). The present study showed a similar rotation for the Eastern Vardar Zone (Avala block, Fig. 10). The Central Vardar Zone must have participated in the above rotation, as it is not only situated in, but sandwiched between the Western Vardar Zone (with obducted ophiolites of Western Vardar Zone) and the Eastern Vardar Zone (Fig. 1). The lower age limit for this event is about 23 Ma, being well constrained in both the wider Rudnik and the Avala areas by the age of the youngest rocks still exhibiting this CW rotation. Estimation for the termination of this rotation needs considerations which involves structural and magnetic markers of the Oligocene and Miocene strain fields and isotope age control, as discussed later.

Two groups of ChRMs of post-folding/tilting age were found for the Upper Cretaceous marls of the Central Vardar Zone. There is no indisputable evidence for the age of their acquisition, but the Oligocene magmatic activity as the agent can be excluded since the overall-mean declinations for both groups (Fig.6) are significantly different from that of the Oligocene magmatites. The most likely times for remagnetization are 1: burial to moderate depth into the subduction zone during the final phase of collision when this process generated metamorphism in the Kopaonik area (~40 Ma, Schefer et al., 2011) 2: a final uplift at the end of Neogene, beginning of Quaternary.

It is interesting to note that the magnetite which is the carrier of the ChRM in the flysch and probably produced from pyrite (e.g. Brothers et al., 1996, Madzin et al., 2021) must have existed during Late Cretaceous-Eocene compression. The evidence for this is that the AARM (anisotropy of the remanence) foliation planes and lineation directions (Fig. 7D and 7E) are sub-parallel to those of the AMS fabrics, i.e. clearly related to the generally E-W oriented compressional strain field (Figs. 8 and 9). This magnetite is likely to have acquired NRM around 40 Ma in an already folded flysch (that explains the negative fold/tilt tests). The question is if the magnetite could have preserved this remanence or the magnetic signal was totally re-set during uplift, during the latest Miocene-Early Pliocene. This problem will be discussed in Section 5.3.

While the ChRMs of the 1st group of localities (Fig. 6F) cover practically the whole segment of the Central Vardar Zone in the surroundings of Belgrade, the four localities belonging to the 2nd group are at a considerable distance from each other (Figs 1, 2 and 6A) and the only common feature of them is that they appear at places where the local tectonics is highly complicated. Thus they can not be considered in terms of regional tectonics.

5.2. Discussion of the results of the structural analysis

The structural analyses allow to define four post-Early Cretaceous deformational episodes.

The first is related to the Late Cretaceous subduction and Paleogene continental collision (Schmid et al., 2020 and references therein). This caused compression perpendicular to the subduction zone (Fig. 8A) and resulted in the Bela Reka Fault, i.e. the basal thrust of the Eastern Vardar Zone over the Central Vardar Zone (Fig. 2). In the same strain field NE-SW oriented right transcurrent faults were also active (Fig. 8B). The ongoing compression during continental collision resulted in the WSW-ward thrust of the Central Vardar and Eastern Vardar Zones over the Western Vardar Zone (Schmid et al., 2008, 2020; Schefer, 2010; Ustaszewski et al., 2010; Toljić et al., 2019). This was accompanied by deformation of the flysch of

the Central Vardar Zone during incorporation in the more internal parts of the orogen (Stojadinović et al., 2017).

As discussed earlier the magnetic fabrics at most localities were formed in the same compressional field as the structural markers of the strain field that prevailed until the end of continental collision (Fig.7 heavy arrows). Poorly defined AMS lineations (Fig. 7, hollow arrows) are interpreted as being due to fold axis reorientation during later tectonic processes.

The onset of continental collision is constrained by the age of the youngest sediments involved in the suture, which are Maastrichtian and Early Paleogene in the Belgrade area (Anđelković, 1973; Toljić et al., 2018). None of the structural data can constrain the termination of the collision However, it was probably co-eval with the youngest metamorphic event, dated 40.9 ± 4.9 Ma in the Studenica metamorphic series of the Kopaonik area (Schefer, 2010), The metamorphism was a result of nappe-stacking related to, and following, the closure of the Central Vardar (suture) Zone. The areas buried by the contraction were exhumed during the Middle-Late Eocene (~34–37 Ma) from below a 4–6 km overburden that was removed by erosion during the coeval contraction (Stojadinović et al., 2017). The final collisional thrusting was completed around 34 Ma.

The deformations continued with NNW-SSE oriented right-lateral transcurrent faults (Fig. 8C), associated with E-W oriented reverse faults (Fig. 8D), both active

in N-S oriented compression. Penetrative brittle shear zones along with local drag folds resulted in steep axes developing along these faults during the strike-slip movements. During transition from perpendicular to oblique compression folds in Upper Cretaceous sediments were partly re-oriented, which is in agreement with orientations of part of the AMS lineations in the areas where re-folding was recorded (Fig. 7). The faults of the Bela Reka system were also reactivated during the same kinematic episode.

It is important to note that the right transcurrent and associated reverse faults were active between ~34 and 30 Ma, i.e. before the Oligocene magmatism (Cvetković et al., 2004) as the strike slip faults were not recorded either in the magmatics or in the Neogene sediments.

The above period was also the time of activation of the dextral transpressional corridor established between the Carpatho-Balkanides and Dinarides (Marović et al., 2007), and coeval with the strike-slip movements in the Kopaonik area (Mladenović et al., 2015) and in the Drina-Ivanjica unit in Western Serbia (Porkoláb et al., 2019). Post-collisional reorientation of the maximum stress axis, from perpendicular to oblique to the strike of the regional structures is explicable as a consequence of rotations of the major lithospheric blocks (Lesić et al.,2011; Mladenović et al., 2015).

The onset of extension in the Vardar Zone started around 30 Ma and lead to the development of the post-Eocene fault pattern and the intrusions of the Lower Oligocene lamprophyre dykes (Fig. 2 and Fig. 8E, F, G) and of the Upper Oligocene latites, quartz-latites, dacites and rhyolites. The faults and dykes were oriented either NE-SW (orogen-parallel extension) or NW-SE (orogen-perpendicular extension). The extension reactivated existing faults, including the Bela Reka Fault, as indicated by field kinematic data (Fig. 8E). Divergent Oligocene-Miocene extension was not restricted to the Vardar Zone, but is a well-known phenomenon in the Pannonian Basin, the peri-Pannonian domain, and the Carpathians (Matenco and Radivojević, 2012; Toljić et al., 2013; Fügenschuh and Schmid, 2005; Krstekanić et al., 2020).

The Neogene sediments, together with their Mesozoic substratum, were only weakly deformed during Pliocene-Quaternary times by NE-SW directed compression (Bada et al., 2007; Rundić et al., 2019).

5.3. Directly observed and inferred rotations and their possible control mechanism

Miocene CW vertical axis rotations are documented in the Eastern and Western Vardar Zones and, inferred due to its tectonic position, for the Central Vardar

Zone. The lower age limit of this rotation is about 23 Ma, being constrained by the youngest igneous rocks that still show this rotation. The termination can be estimated by comparison of the orientation of the Oligocene-Early Miocene strain field in the Belgrade area (Fig. 8) on one hand, with the AMS lineations imprinted during extensional unroofing of the Kopaonik, Drenje and Polumir plutons, on the other hand. In the Belgrade area the direction of the extension is dominantly NE-SW in present coordinates (Fig.8). In the Kopaonik area, AMS (stretching) lineations related to extension are also NE-SW oriented in the older I-type plutons. The extension responsible for the very intensive AMS fabrics (Lesić et al., 2013) was probably connected to the unroofing which terminated around 21 Ma (Schefer et al., 2011). Ductile extensional deformation was also responsible for the AMS fabrics of the Polumir pluton, emplaced around 18 Ma. In this pluton the AMS lineation is directed N-S. The implication is that the extension direction must have been close to N-S throughout the Oligocene and earliest Miocene and the different orientations of the AMS lineations in the I-type and S-type plutons is the consequence of the paleomagnetically constrained CW vertical axis rotation (Lesić et al., 2019 and the present study).

The CW rotation measured directly for the Kopaonik and Rudnik areas, as well as for the Avala region, and inferred for the Central Vardar Zone seems to coincide with the initial opening of the Pannonian Basin, as manifested by the deposition

of lacustrine Lower Miocene sediments in the Belgrade area (e.g. Marović et al., 2002). The regional extensional tectonic evolution of the Pannonian basin started between the Dinaridic and the Carpathian slabs (Matenco and Radivojević, 2012; Stojadinović et al., 2013 and references therein), but after the detachment of the Dinaridic slab (Andrić et al., 2018), it was primarily governed by the rollback of the Carpathian slab (Horváth et al., 2015). Some authors favour the rollback of the Carpathian oceanic lithosphere as being the mayor control mechanism of the Oligocene-Miocene extension in the areas of the Pannonian Basin, Dinarides and Southern Carpathians, including the suture zone (Ustaszewski et al., 2010; Stojadinović et al., 2013; Toljić et al., 2013; Fodor et al., 2021; Löwe et al., 2021). The influence of this extension is recognizable further south along the peri-Pannonian domain (Erak et al., 2017; Mladenović et al., 2015). The rigid Moesia also played an active role in the shaping the regional tectonic pattern, the partitioning of deformation and gradual shift and rotation of tectonic units and structures (Krstekanić et al., 2020, 2021).

As the paleomagnetic results suggest the extension, was accompanied with CW rotation, in the Pannonian Basin S of the Mid-Hungarian shear zone (in contrast to the CCW rotations to the N of it) and also the Carpathian-Dinaridic orogenic system (Fig. 11). The retreat of the subducted plate, and extensional opening of the southern Pannonian Basin, are accommodated by the ingression of the Tisza-

Dacia block to the east, and by the migration of the half-graben and depocenters in same direction (Matenco and Radivojević, 2012; Fodor et al., 2021).

Due to its position between the Eastern and Western Vardar Zones, the Central Vardar Zone must have participated in the 30-34° Miocene vertical axis CW rotation, but such rotation is not reflected in the overall mean declination of the 1st group of data from the Upper Cretaceous flysch. This declination is 356°, which in case of positive fold/tilt test would imply about 34-38° pre-Oligocene CCW rotation of the Belgrade segment of the Central Vardar Zone. However, the test is negative and since the overall mean direction based on the number of localities isnot significantly different statistically from a paleomagnetic direction expected for the study area between 10 and 0 Ma, it is logical to interpret it as a young overprint. For the same data set, statistical calculations based on the number of samples, as it is more and more popular among paleomagnetists, reduce by about half the statistical error (Fig. 12, Supplementary Table 1). In this case, the difference becomes significant.

Independently of the statistical considerations, there are paleomagnetic and structural observations which point to the possibility of an alternative interpretation, which is retaining the magnetization acquired around 40 Ma during shallow burial (see Chapter 5.1). These are 1: spread of the declinations of

the individual localities between 315 and 32° (all normal polarity, except one Table 1, locality 1). The fan-like distribution can be connected to tectonic movements that resulted in the highly complicated pre-Oligocene structure of the Vardar Zone (Fig. 13) 2: the paleolatitude fitting perfectly the expected paleolatitude at the study area expected from the reference paleolatitudes from both Africa and stable Europe (Fig. 12). 3: according to the generally accepted tectonic model of the Vardar Zone, its whole assemblage was emplaced on top of the Drina Ivanjica unit, which was thrusted over Adriatic elements in its turn (Fig. 14), therefore participated in its post-Cretaceous CCW rotation. This rotation could be responsible for systematic right lateral Early Oligocene strike-slip faulting (Fig. 8C), which was also recognized in the southern part of the Vardar Zone (Marović et al., 2007), but also in Drina-Ivanjica Unit (Porkoláb et al., 2019). Thus, the CCW rotation of the Central Vardar Zone during the Paleogene, inferred from the alternative interpretation of the relevant data is in line with the generally accepted tectonic model, and therefore deserves attention.

6. Conclusions

Integrated paleomagnetic and kinematic investigations in the Belgrade surroundings indicate complex poly-phase deformations and vertical axis rotations in this area. The paleomagnetic results from the Eastern Vardar Zone, together with earlier published ones from the Western Vardar Zone, document a ~30° CW vertical axis rotation between 23 (21) and 18 Ma. The lower limit is constrained by the youngest age of the magmatic rocks intruded in both zones during the Late Oligocene – Early Miocene extension. The upper age limit is derived from the difference in the directions of the stretching lineations between I-type and S-type plutons of the Kopaonik area (Western Vardar Zone). Due to its tectonic position between the Western and Eastern Vardar Zones, the Central Vardar Zone must have participated in that rotation.

The extension and the CW rotation in the Vardar Zone, is connected to the post-subduction dynamics of the Dinaridic and Carpathian slabs, and, following the detachment of the former, to the roll-back of Carpathians oceanic lithosphere.

The tectonic interpretation of the paleomagnetic directions for the Upper Cretaceous flysch from the Central Vardar Zone are less straightforward. The main reason is that two groups of paleomagnetic directions were observed, both

of post-folding/tilting age. One group, consisting of four localities at considerable distance from each other, must have local significance. The other, containing 15 localities, practically covering the whole Belgrade segment of the Central Vardar Zone, has an overall-mean declination close to the present north, but shallower than the Late Miocene inclination. Taking into account the statistical error of the overall mean direction based on localities, the results can be interpreted as remagnetization during Late Neogene uplift. However, an alternative interpretation is possible by the perfect fit of the overall-mean inclination to a remagnetization age of about 40 Ma and the fan-like distributed declinations of the individual localities. The spread of the declinations can be the consequence of the activity of the Early Oligocene abundant right lateral strike slip faults. Such interpretation is, in fact, in harmony with the pre-Late Oligocene tectonic model of the region. According to the generally accepted model, the main Zones (and tectonic slices within the Zones) were thrust from E to W, eventually over Adriatic elements during Paleogene compression. The whole assembly was affected by the post-Cretaceous CCW rotation of Adria, held responsible for the widely observed right lateral strike-slip faulting in the Vardar Zone. It stands to reason to assume that the main tectonic zones and the tectonic slices inside them were affected by decreasing magnitude of rotation with increasing distance from the Adriatic elements.

Acknowledgements

Revisions by two anonymous referees are thankfully acknowledged. Emő Márton thanks Don Tarling for polishing the English of the paper and his suggestions for improving it. This work was supported by the National Development and Innovation Office of Hungary, project K 128625, and by the Ministry of Education and Science of the Republic of Serbia, projects 176015 and 176016.

References

Andrić, N., Vogt, K., Matenco, L., Cvetković, V., Cloetingh, S. and Gerya, T., (2018). Variability of orogenic magmatism during continental collision: A numerical modelling approach. Gondwana Research, 56, 119-134. doi: 10.1016/j.gr.2017.12.007

Anđelković, M., (1973). Geology of Mesozoic vicinity of Belgrade (in Serbian). Annales Geologiques de la Peninsule Balkanique 38, 1–136.

Bada, G., Horváth, F., Dovenyi, P., Szafian, P., Windhoffer, G. and Cloetingh, S., (2007). Present-day stress field and tectonic inversion in the Pannonian basin. Global and Planetary Change, 58, 165 – 180.

Balla, Z., Márton, E. and Gulácsi, Z., (2011). The age of the Cretaceous subvulcanic bodies from South Transdanubia (Hungary), based on palaeomagnetic measurements (in Hungarian). Földtani Közlöny, 141, 233–250.

Bordás, R., (1990). Aniso – anisotropy program package for IBM PC. ELGI, Budapest.

Bragin, N.Y., Bragina, Lj.G., Djerić, N. and Toljić, M., (2011). Triassic and Jurassic radiolarians from sedimentary blocks of ophiolite mélange in the Avala Gora area (Belgrade surroundings, Serbia). Stratigraphy and Geological Correlation, 19, 6, 631 640.

Brothers, L.A., Engel, M.H. and Elmore, R.D., (1996). The late diagenetic conversion of pyrite to magnetite by organically complexed ferric iron. Chemical Geology, 130, 1–14.

Butler, R.F., (1992). Paleomagnetism: magnetic domains to geological terranes. Blackwell Scientific Publications, Oxford, p 319.

Chadima, M. and Jelínek, V., (2008). Anisoft 4.2.—Anisotropy data browser. Contributions to Geophysics and Geodesy, 38, p 41.

Chadima, M., Hrouda, F. and Jelínek, V., (2018). Anisoft 5.1—Advanced treatment of magnetic anisotropy data. Geophysical Research Abstracts 20, EGU-2018-15017.

Cvetkov, V., Lesić, V., Vasković, N., (2012). New paleomagnetic results for Tertiary magmatic rocks of Fruška Gora, Serbia. Annales geologiques de la Peninsule Balkanique, 73, 99–108.

Cvetković, V., Prelević, D., Downes, H., Jovanović, M., Vaselli, O. and Pécskay, Z., (2004). Origin and geodynamic significance of Tertiary postcollisional basaltic magmatism in Serbia (central Balkan Peninsula). Lithos, 73, 3-4, 161-186.

Cvetković, V., Pécskay, Z., Šarić, K., (2013). Cenozoic igneous tectonomagmatic events in the Serbian part of the Balkan Peninsula: inferences from K/Ar geochronology. Geologia Acta Vulcanologica, 25, 111–120.

Debiche, M.G., Watson, G.S., (1995). Confidence limits and bias correction for estimating angles between directions with application to paleomagnetism: Journal of Geophysical Research, v. 100, no. B12, p. 22405–22429, https://doi.org/10.1029/92JB01318.

Dimitrijević, M.D., (1997). Geology of Yugoslavia Beograd, Geoinstitut-Barex, p. 187.

Enkin, R., (2003a). The direction–correction tilt test: an all-purpose tilt / fold test for paleomagnetic studies. Earth and Planetary Science Letters, 212, 151–166.

Enkin, R., (2003b). PMGSC Paleomagnetism Data Analysis, v 4.2: Sidney, Geological Survey of Canada.

Erak, D., Matenco, L., Toljić, M., Stojadinović, U., Andriessen, P.A.M., Willingshofer, E. and Ducea, M.N., (2017). From nappe stacking to extensional detachments at the contact between the Carpathians and Dinarides – The Jastrebac Mountains of Central Serbia. Tectonophysics, 710–711, 162–183.

Fisher, R.A., (1953). Dispersion on a sphere. Proceedings of the Royal Society London, 217, 295–305.

Fodor, L., Balázs, A., Csillag, G., Dunkl, I., Héja, G., Jelen, B., Kelemen, P., Kövér, S., Németh, A., Nyíri, D., Selmeczi, I., Trajanova, M., Vrabec, M., Vrabec, M., (2021). Crustal exhumation and depocenter migration from the Alpine orogenic margin towards the Pannonian extensional back-arc basin controlled by inheritance, Global and Planetary Change, Volume 201, 103475, https://doi.org/10.1016/j.gloplacha.2021.103475.

Fügenschuh, B. and Schmid, S.M., (2005). Age and significance of core complex formation in a very curved orogen: evidence from fission track studies in the South Carpathians (Romania). Tectonophysics, 404, 33–53.

Grohmann, C.H. and Campanha, G.A., (2010). OpenStereo: Open Source, Cross-Platform Software for Structural Geology Analysis. American Geophysical Union, Fall Meeting 2010, abstract id. IN31C-06, San Francisco, Calif., 13-17 Dec.

Horváth, F., (1993). Towards a kinematic model for the formation of the Pannonian basin. Tectonophysics, 226, 333–357.

Horváth, F., Musitz, B., Balázs, A., Végh, A., Uhrin, A., Nádor, A., Koroknai, B., Pap, N., Tóth, T. and Wórum, G., (2015). Evolution of the Pannonian basin and its geothermal resources. Geothermics, 53, 328-352.

Hrouda, F., (1994). A technique for the measurement of thermal changes of magnetic susceptibility of weakly magnetic rocks by the CS-2 apparatus and KLY-2 Kappabridge. Geophysical Journal International, 118, 604-612.

Jelínek, V., (1977). The statistical theory of measuring anisotropy of magnetic susceptibility of rocks and its application. Geofyzika, Sp, Brno.

Jelínek, V., (1978). Statistical processing of anisotropy of magnetic susceptibility measured on groups of sediments. Studia Geophys Geodynamics, 22, 50–62.

Jelínek, V., (1981). Characterization of magnetic fabric of rocks. Tectonophysics, 79, T63–T67.

Karamata, S., (2006). The geological development of the Balkan Peninsula related to the approach, collision and compression of Gondwana and Eurasian units. In A.H.F. Robertson & D. Mountrakis (Ed.), Tectonic development of the Eastern Mediterranean region. Geological Society London, Special Publication, 260, 155–178.

Kirschvink, J.L., (1980). The least-squares line and plane and the analysis of paleomagnetic data. Geophysical Journal of the Royal Astronomical Society, 62, 699–718.

Krs, M., Krsová M., Chvojka R. and Potfaj M., (1991). Paleomagnetic investigations of the flysch belt in the Orava region, Magura unit, Czechoslovak Western Carpathians. Geologické práce, Správy, 92, 135–151.

Krstekanić, N., Matenco, L., Toljić, M., Mandić, O., Stojadinović, U. and Willingshofer, E., (2020). Understanding partitioning of deformation in highly arcuate orogenic systems: inferences from the evolution of the Serbian Carpathians. Glob. Planet. Chang., 195, 103361, https://doi.org/10.1016/j.gloplacha.2020.103361

Krstekanić, N., Willingshofer, E., Broerse, T., Matenco, L., Toljić, M. and Stojadinović, U., (2021). Analogue modelling of strain partitioning along a

curved strike-slip fault system during backarc-convex orocline formation: Implications for the Cerna-Timok fault system of the Carpatho-Balkanides. Journal of Structural Geology, 149, 104386, https://doi.org/10.1016/j.jsg.2021.104386

Lesić, V., Márton, E. and Cvetkov, V., (2007). Paleomagnetic detection of Tertiary rotations in the Southern Pannonian Basin (Fruška Gora). Geologica Carpathica, 58, 185–193.

Lesić, V., Márton, E., Cvetkov, V. and Tomić, D., (2013). Magnetic anisotropy of Cenozoic igneous rocks from the Vardar zone (Kopaonik area, Serbia). Geophysical Journal International, 193, 1182–1197.

Lesić, V., Márton, E., Cvetkov, V. and Tomić, D., (2015). Paleomagnetic evidence for post-collisional Miocene clockwise rotation in the Serbian segment of the Vardar Zone and the Danubicum. 26th IUGG General Assembly, Abstracts IUGG-1324.

Lesić, V., Márton, E., Jovanović, D., Luković, A. and Cvetkov, V., (2018). Paleomagnetic results from Timok magmatic complex, Eastern Serbia. In: M. Ganić, V. Cvetkov, P. Vulić, D. Đurić, U. Đurić (eds) 17th Serbian Geological Congress, Book of Abstracts, Serbian Geological Society, Belgrade, 747-751.

Lesić, V., Márton, E., Gajić, V., Jovanović, D. and Cvetkov, V., (2019). Clockwise vertical-axis rotation in the West Vardar zone of Serbia: tectonic implications. Swiss Journal of Geosciences, 112, 199–215.

Löwe, G., Schneider, S., Sperner, B., Balling, F., Pfänder, J.A. and Ustaszewski, K., (2021). Torn Between Two Plates: Exhumation of the Cer Massif (Internal Dinarides) as a far-field effect of Carpathian slab rollback Inferred from 40Ar/39Ar dating and cross section balancing. Tectonics, 40, e2021TC006699. https://doi.org/10.1029/2021TC006699

Lowrie, W., (1990). Identification of feromagnetic minerals in a rock by coercitive and unblocking temperature properties. Geophysical Research Letters, 17, 159–162.

Madzin, J., Márton, E., Starek, D., Mikuš, T., (2021). Magnetic fabrics in the turbidite deposits of the Central Carpathian Paleogene Basin in relation to sedimentary and tectonic fabric elements. Geologica Carpathica, 72, 2, 134–154, https://doi.org/10.31577/GeolCarp.72.2.4

Marović, M., Djoković, I., Pešić, L., Radovanović, S., Toljić, M. and Gerzina, N., (2002). Neotectonics and seismicity of the southern margin of the

Pannonian basin in Serbia. EGU Special Publication, 277–295. doi: 10.5194/smsps-3-277-2002

Marović, M., Djoković, I., Toljić, M., Milivojević, J. and Spahić, D., (2007). Paleogene-Early Miocene deformations of Bukulja-Venčac crystalline (Vardar Zone, Serbia). Ann. Geol. Peninsule Balkanique 68, 9–20.

Márton, E., (1986). Paleomagnetism of igneous rocks from the Velence Hills and Mecsek Mountains. Geophysical Transactions, 32, 83–145.

Márton, E., (2000). The Tisza megatectonic unit in the light of paleomagnetic data. Acta Geologica Hungarica, 43/3, 329–343.

Márton, E., (2020) Last scene in the large scale rotations of the Western Carpathians as reflected in paleomagnetic constraints. Geology, Geophysics and Environment, 46/2, 109–133. https://doi.org/10.7494/geol.2020.46.2.109

Márton, E. and Fodor, L., (1995). Combination of palaeomagnetic and stress data - a case study from North Hungary. Tectonophysics, 242, 99–114.

Márton, E. and Fodor, L., (2003). Tertiary paleomagnetic results and structural analysis from the Transdanubian Range (Hungary); sign for rotational disintegration of the Alcapa unit. Tectonophysics, 363, 201–224.

Márton, E. and Márton, P., (1983). A refined apparent polar wander curve for the Transdanubian Central Mountains and its bearing on the Mediterranean tectonic history. Tectonophysics, 98, 43–57.

Márton, E. and Márton, P., (1996) Large scale rotations in North Hungary during the Neogene as indicated by palaeomagnetic data. In: Morris, A. & Tarling, D.H. (eds), Palaeomagnetism and Tectonics of the Mediterranean Region, Geological Society Special Publication, 105, 153-173.

Márton, E., Tischler, M., Csontos, L., Fügenschuh, B. and Schmid, S.M., (2007). The contact zone between ALCAPA and Tisza-Dacia megatectonic units of Northern Romania in the light of new paleomagnetic data. Eclogae geologicae Helvetiae, 100, 109–124.

Márton, E., Ćosović, V., Moro, A. and Zvocak, S., (2008). The motion of Adria during the Late Jurassic and Cretaceous: New paleomagnetic results from stable Istria. Tectonophysics, 454/1-4, 44–53.

Márton, E., Fodor, L., Kövér, Sz., Lesić, V., Đerić, N. and Gerzina Spajić, N., (2018). New paleomagnetic results from the Inner Dinarides, SW Serbia. In: M. Ganić, V. Cvetkov, P. Vulić, D. Đurić, U. Đurić (eds) 17th Serbian Geological Congress, Book of Abstracts, (ISBN:978-86-86053-20-6) Serbian Geological Society, Belgrade, 752-756.

Matenco, L. and Radivojević, D., (2012). On the formation and evolution of the Pannonian Basin: Constraints derived from the structure of the junction area between the Carpathians and Dinarides. Tectonics 31, TC6007. DOI: 10.1029/2012TC003206

McFadden, P.L. and McElhinny, M. W., (1990). Classification of the reversal test in palaeomagnetism. Geophysical Journal International, 103, 725–729.

Mladenović, A., Trivić, B. and Cvetković, V., (2015). How tectonics controlled post-collisional magmatism within the Dinarides: Inferences based on study of tectono-magmatic events in the Kopaonik Mts. (Southern Serbia). Tectonophysics, 646, 36–49.

Ortner, H., Reiter, F. and Acs, P., (2002). Easy handling of tectonic data: the programs TectonicVB for Mac and TectonicsFP for Windows. Comput. Geosci., 28, 1193–1200.

Pamić, J., (2002). The Sava-Vardar Zone of the Dinarides and Hellenides versus the Vardar Ocean. Eclogae Geologicae Helvetiae, 95 (1), 99–113.

Panaiotu, C., (1998). Paleomagnetic constraints on the geodynamic history of Romania. In: Ioane, D. (ed.): Monograph of Southern Carpathians. Reports on Geodesy, 7, 205–216.

Panaiotu, C. G., Panaiotu, C. E., and Lazar, I., (2012). Remagnetization of Upper Jurassic limestones from the Danubian Unit (Southern Carpathians, Romania): Tectonic implications. Geologica Carpathica, 63, 453–461.

Parma, J., Hrouda, F., Pokorný, J., Wohlgemuth, J., Suza, P., Šilinger, P. and Zapletal, K., (1993). A technique for measuring temperature dependent susceptibility of weakly magnetic rocks. EOS, Trans. Am. Geophys. Un. Spring meeting 1993, 113.

Pătraşcu, S., Bleahu, M. and Panaiotu, C., (1990). Tectonic implications of paleomagnetic research into Upper Cretaceous magmatic rocks in the Apuseni Mountains, Romania. Tectonophysics, 180, 309–322.

Porkoláb, K., Kövér, S., Benkó, Z., Héja, G.H., Fialowski, M., Soós, B., Gerzina Spajić, N., Đerić, N. and Fodor, L., (2019). Structural and geochronological constraints from the Drina-Ivanjica thrust sheet (Western Serbia): implications for the Cretaceous–Paleogene tectonics of the Internal Dinarides. Swiss J. Geosci., 112, 217–234. https://doi.org/10.1007/s00015-018-0327-2

Rundić, Lj., Ganić, M., Knežević, S., Radivojević, D. and Radonjić, M., (2019). Stratigraphic implications of the Mio-Pliocene geodynamics in the area of

Mt. Avala: new evidence from Torlak Hill and Beli Potok (Belgrade, Serbia). Geologia Croatica, 72/2, 109-128. https://doi.org/10.4154/gc.2019.11

Schefer, S., (2010). Tectono-metamorphic and magmatic evolution of the Internal Dinarides (Kopaonik area, southern Serbia) and its significance for the geodynamic evolution of the Balkan Peninsula. (PhD thesis). University of Basel, Switzerland. p 234.

Schefer, S., Cvetković, V., Fügenschuh, B., Kounov, A., Ovtcharova, M., Schaltegger, U. and Schmid, S., (2011). Cenozoic granitoids in the Dinarides of southern Serbia: age of intrusion, isotope geochemistry, exhumation history and significance for the geodynamic evolution of the Balkan Peninsula. International Journal of Earth Sciences (Geological Rundschau), 100, 1181-1206.

Schmid, S.M., Bernoulli, D., Fügenschuh, B., Matenco, L., Schefer, S., Schuster, R., Tischler, M. and Ustaszewski, K., (2008). The Alpine – Carpathian – Dinaric orogenic system: Correlation and evolution of tectonic units. Swiss Journal of Geoscience, 101, 139–183.

Schmid, S.M., Fügenschuh, B., Georgiev, N., Kounov, A., Maţenco, L., Nievergelt, P., Oberhänsli, R., Pleuger, J., Schefer, S., Schuster, R., Tomljenovic, B., Ustaszewski, K. and van Hinsbergen, D.J.J., (2020). Tectonic units of the Alpine collision zone between Eastern Alps and western Turkey. Gondwana Research, 78, 308-374. https://doi.org/10.1016/j.gr.2019.07.005

Sokol, K., Prelević, D., Romer, R.L., Božović, M., van den Bogaard, P., Stefanova, E., Kostić, B. and Čokulov, N., (2020). Cretaceous ultrapotassic magmatism from the Sava-Vardar Zone of the Balkans. Lithos, 354-355. https://doi.org/10.1016/j.lithos.2019.105268.

Stojadinović, U., Matenco, L., Andriessen, P.A.M., Toljić, M. and Foeken, J.P.T., (2013). The balance between orogenic building and subsequent extension during the Tertiary evolution of the NE Dinarides: Constraints from low-temperature thermochronology. Global and Planetary Change, 103, 19-38.

Stojadinović, U., Matenco, L., Andriessen, P., Toljić, M., Rundić, L. and Ducea, M.N., (2017). Structure and provenance of Late Cretaceous–Miocene sediments located near the NE Dinarides margin: Inferences from kinematics of orogenic building and subsequent extensional collapse. Tectonophysics, 710–711, 184-204. https://doi.org/10.1016/j.tecto.2016.12.021

Thébault, E., Finlay, C. C., Beggan, C. D., Alken, P., Aubert, J., Barrois, O., Bertrand, F., Bondar, T., Boness, A, Brocco, L., Canet, E., Chambodut, A., Chulliat, A., Coïsson, P., Civet, F., Du, A., Fournier, A., Fratter, I., Gillet, N., Hamilton, B.,

Hamoudi, M., Hulot, G., Jager, T., Korte, M., Kuang, W., Lalanne, X., Langlais, B., Léger, J-M., Lesur, V., Lowes, F. J., Macmillan, S., Mandea, M., Manoj, C., Maus, S., Olsen, N., Petrov, V., Ridley, V., Rother, M., Sabaka, T. J., Saturnino1, D., Schachtschneider, R., Siro, O., Tangborn, A., Thomson, A., Tøffner-Clausen, L., Vigneron, P., Wardinski, I. and Zvereva, T., (2015). International Geomagnetic Reference Field: the 12th generation. Earth, Planets and Space, 67, article no 79.

Toljić, M., Matenco, L., Ducea, M.N., Stojadinović, U., Milivojević, J. and Djerić, N., (2013). The evolution of a key segment in the Europe–Adria collision: the Fruška Gora of northern Serbia. Glob. Planet. Chang., 103, 39–62.

Toljić, M., Matenco, L., Stojadinović, U., Willinshofer, E. and Ljubović-Obradović, D., (2018). Understanding fossil fore-arc basins: Inferences from the Cretaceous Adria-Europe convergence in the NE Dinarides. Global and Planetary Change, 171, 167-184.

Toljić, M., Stojadinović, U. and Krstekanić, N., (2019). Vardar Zone: New insights into the tectono-depositional subdivision. Proceedings of the II Congress of Geologists of Bosnia and Herzegovina, October 2-4, Laktaši, Bosnia and Herzegovina, 60-73.

Toljić, M., Glavaš-Trbić, B., Stojadinović, U., Krstekanić, N. and Srećković-Batoćanin, D., (2020). Geodynamic interpretation of the Late Cretaceous syn-depositional magmatism in central Serbia: Inferences from biostratigraphic and petrological investigations. Geologica Carpathica, 71, 6, 526 – 538. https://doi.org/10.31577/GeolCarp.71.6.4

Ustaszewski, K., Kounov, A., Schmid, S., Schaltegger, U., Krenn, E., Frank, W. and Fügenschuh, B., (2010). Evolution of the Adria-Europe plate boundary in the northern Dinarides: From continent-continent collision to back-arc extension. Tectonics, 29, 1-34.

Torsvik, T. H., Van der Voo, R., Preeden, U., Mac Niocaill, C., Steinberger, B., Doubrovine, P. V., Van Hinsbergen, D. J. J., Domeier, M., Gaina, C., Tohver, E., Meert, J. G., Mccausland, P. J. A. and Cocks, L. R. M., (2012). Phanerozoic polar wander, paleogeography and dynamics. Earth Science Review, 114, 325-368.

Vasković, N. and Matović, V., (1996). The Tertiary volcanic rocks from Mt. Avala. Annales geologiques de la Peninsule Balkanique, 60, 1, 391-404.

Zijderveld, J.D.A., (1967). A.C. demagnetization of rocks: Analysis of results. In: Methods in palaeomagnetism, eds. D.V. Collinson, K.M. Creer and S.K. Runcorn, Elsevier, Amsterdam, pp. 254–286.

Supplement 1

The tectonic units defined by the different authors can be correlated in the following way. The Jadar-Kopaonik unit and Western Vardar ophiolitic unit of Schmid et al. (2008) are correlated with the Vardar Zone western oceanic basin of Karamata (2006) and the western parts of External Vardar Subzone of Dimitrijević (1997). The Eastern Vardar ophiolitic unit of Schmid et al. (2008) are correlated with the Main basin of the Vardar Ocean (Karamata, 2006) and the Central Vardar Subzone of Dimitrijević (1997). The Sava suture zone of Schmid (2008) is partly correlatable with the Kopaonik block and ridge unit of Karamata (2006), and partly with the eastern segments of the External Vardar Subzone of Dimitrijević (1997). The Internal Vardar Subzone (Dimitrijević, 1997) spatially and lithostratigraphically represents a segment of the tectonized western periphery of the Serbomacedonian Massif.

References

Dimitrijević, M.D., (1997). Geology of Yugoslavia Beograd, Geoinstitut-Barex, p. 187.

Karamata, S., (2006). The geological development of the Balkan Peninsula related to the approach, collision and compression of Gondwana and Eurasian units. In A.H.F. Robertson & D. Mountrakis (Ed.), Tectonic development of the Eastern Mediterranean region. Geological Society London, Special Publication, 260, 155–178.

Schmid, S.M., Bernoulli, D., Fügenschuh, B., Matenco, L., Schefer, S., Schuster, R., Tischler, M. and Ustaszewski, K., (2008). The Alpine – Carpathian – Dinaric orogenic system: Correlation and evolution of tectonic units. Swiss Journal of Geoscience, 101, 139–183.

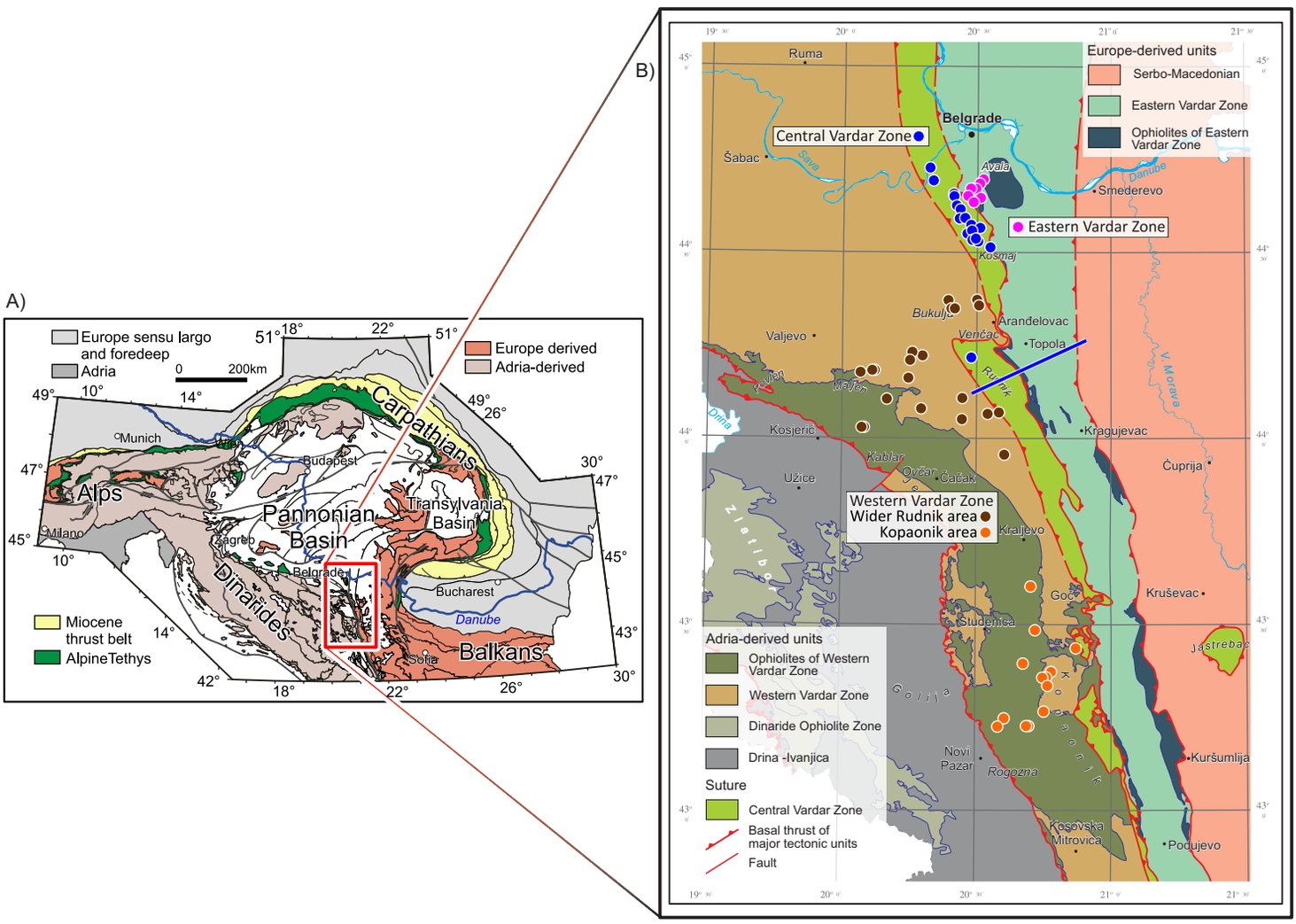

Fig. 1. A) Tectonic map of the Alps – Carpathians – Dinaridic system (simplified after Schmid et al., 2008); B) Tectonic map of the contact area between Europe- and Adria- derived units around and south of Belgrade with the paleomagnetic sampling localities (modified after Toljić et al., 2019). The blue line indicates the position of the detailed cross-section.

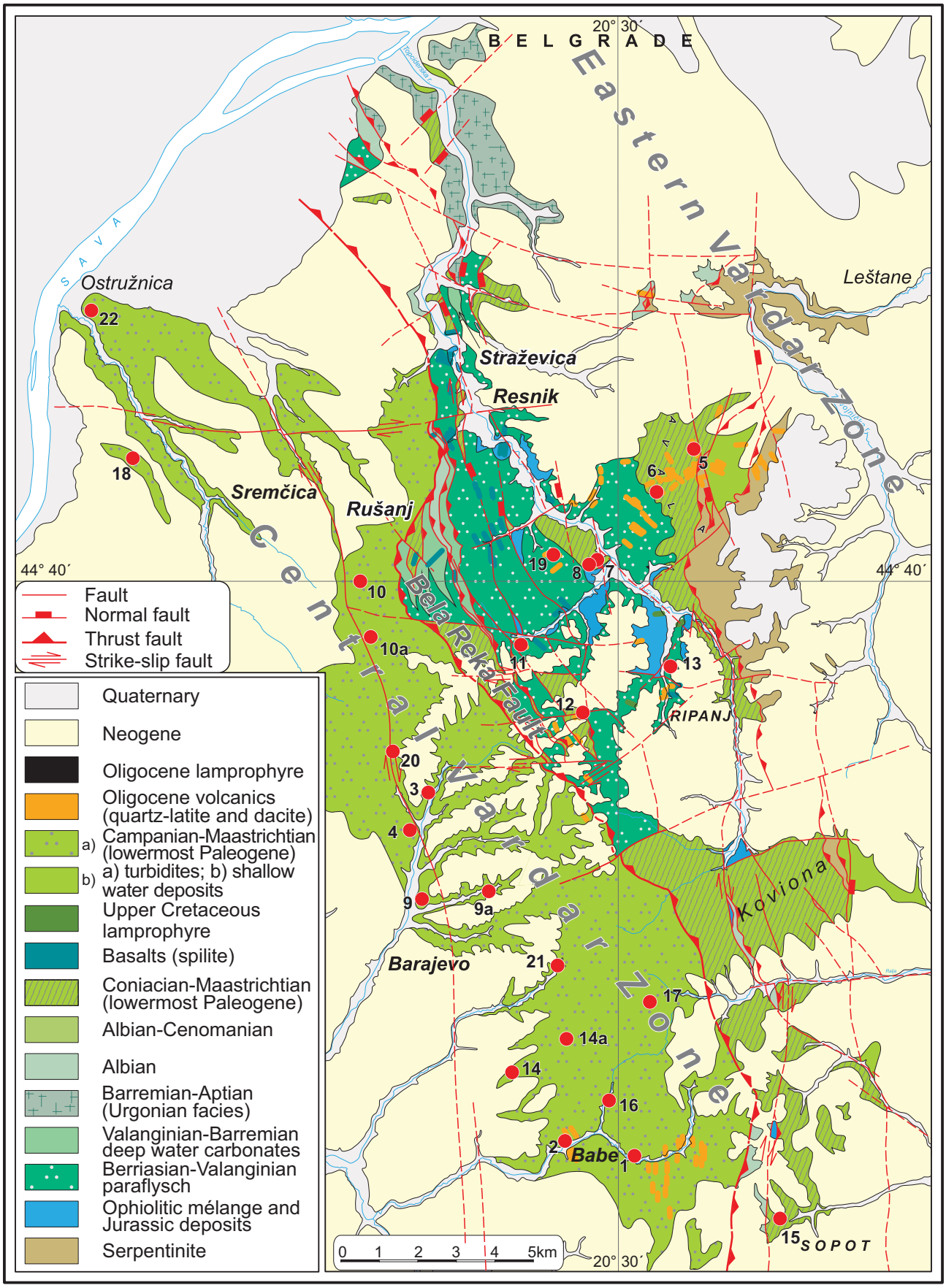

Fig. 2. Simplified geological map of the Belgrade area (modified after Toljić et al., 2018). The Bela Reka Fault separates the Upper Cretaceous flysch of the Central Vardar Zone and the Cretaceous sediments plus obducted ophiolites of the Eastern Vardar Zone. Paleomagnetic sampling localities/sites (1-22) are shown as dots. The identification numbers are used throughout the paper.

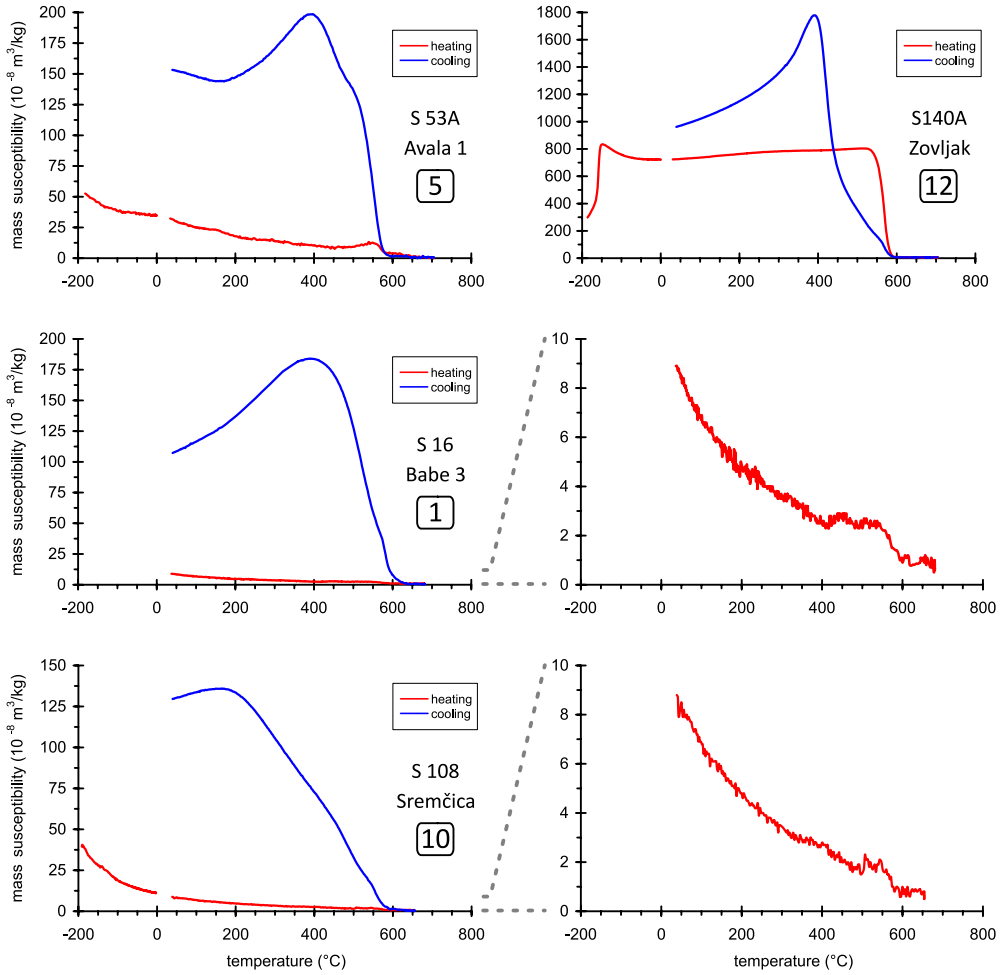

Fig. 3. Temperature vs. magnetic susceptibility curves from selected sites/ localities. Site 5 is a quartz-latite dyke, site 12 is a latite dyke from the Avala area, Eastern Vardar Zone, both identifying magnetite (Curie points 577°C and 580°C respectively, very close to the 575°C Curie point of stöchiometric magnetite) as the magnetic mineral, with a substantial contribution of paramagnetic minerals in the first case (well visible paramagnetic hyperbola, estimated paramagnetic contribution to susceptibility is 96%. Localities 1 and 10 are Upper Cretaceous marls from the Central Vardar Zone with subordinate magnetite (Curie points are 588°C and 582°C, respectively. These are clearly visible in the magnified heating curves on the right side of the respective diagrams) In both cases 94% of the susceptibility is connected to paramagnetic minerals (documented by the paramagnetic hyperbola in both cases). Estimation of paramagnetic contribution: method by Hrouda (1994).

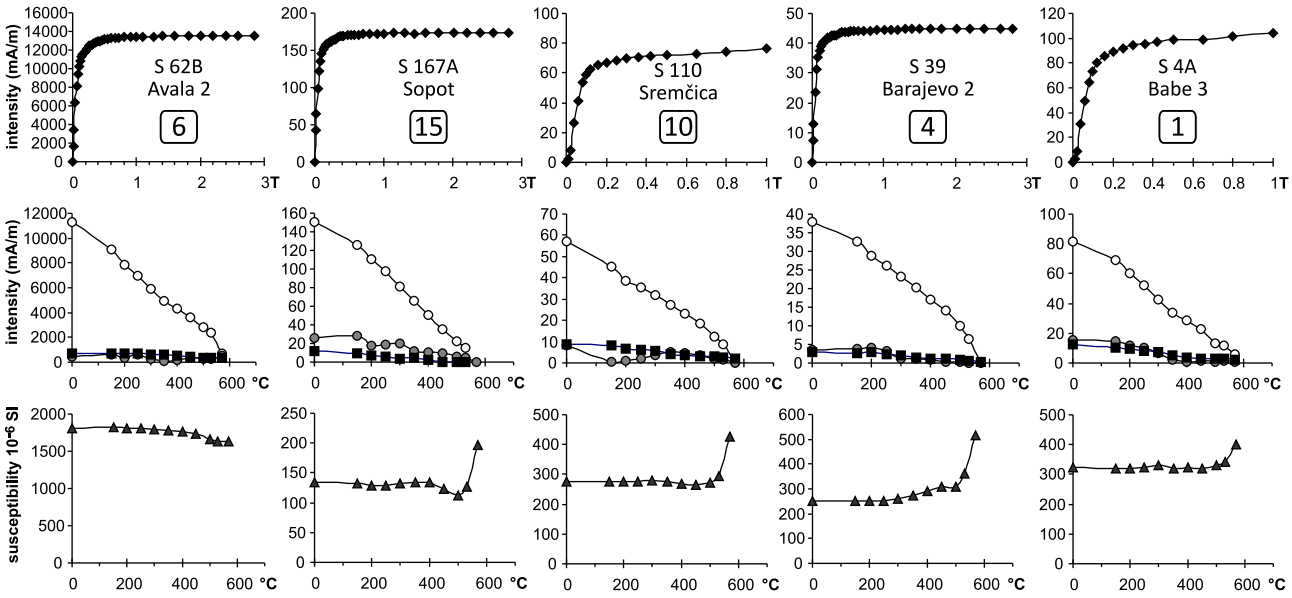

Fig. 4. Identification of the magnetic minerals (method by Lowrie, 1990) in Upper Cretaceous sediments from the Belgrade area. Locality 6 is a shallow water carbonate from the Avala Mts, localities 10, 4, 1 are marls from the Central Vardar Zone and locality 15 is marl close to the Bela Reka Fault. From top to bottom: IRM acquisition, thermal demagnetization of the 3-component IRM, susceptibility during heating. The components of the IRM were acquired in fields of 2.8 or 1.0 T (squares), 0.36 T (full circles) and 0.12 T (open circles). The dominant soft component decays by the Curie-point of magnetite.

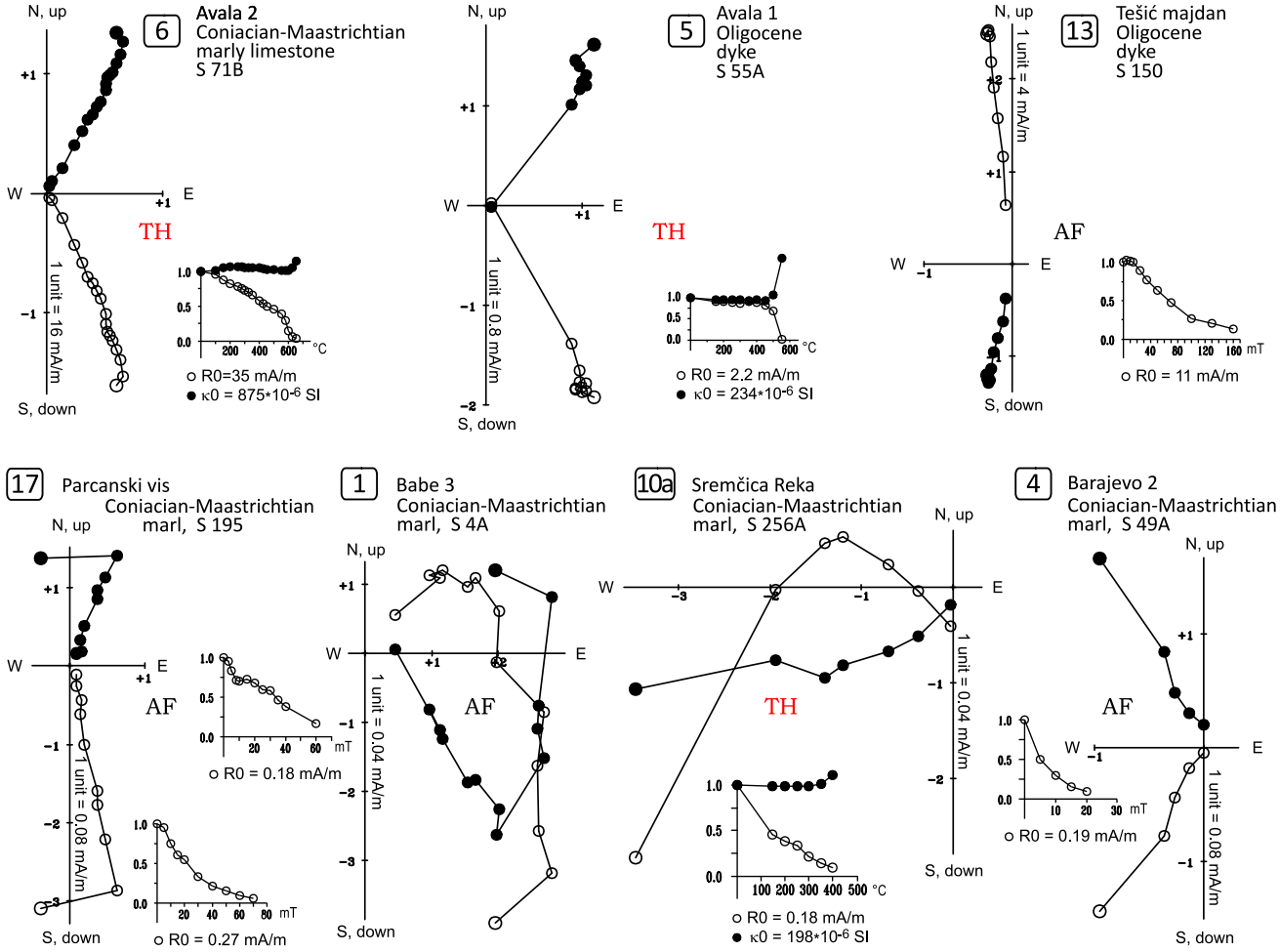

Fig. 5. Typical demagnetization curves for igneous and sedimentary rocks from the Belgrade area. Shallow water carbonates (locality 6) and Oligocene dykes (sites 5 and 13) from the Avala area have typically single component NRM. Some of the Upper Cretaceous marls from the Central Vardar Zone exhibit basically single component (localities 14 and 4); others are composite NRMs (localities 1 and 10a). Key: Zijderveld diagrams (Zijderveld, 1967) are oriented in geographically and, in case of AF demagnetization they are accompanied by intensity (circles) versus demagnetizing field diagrams, and by NRM intensity (circles)/susceptibility (dots) v.s. temperature diagrams, when the method is thermal (TH) demagnetization. In the Zijderveld diagrams full dots are the projections of the NRM vector onto the horizontal; circles: into the vertical.

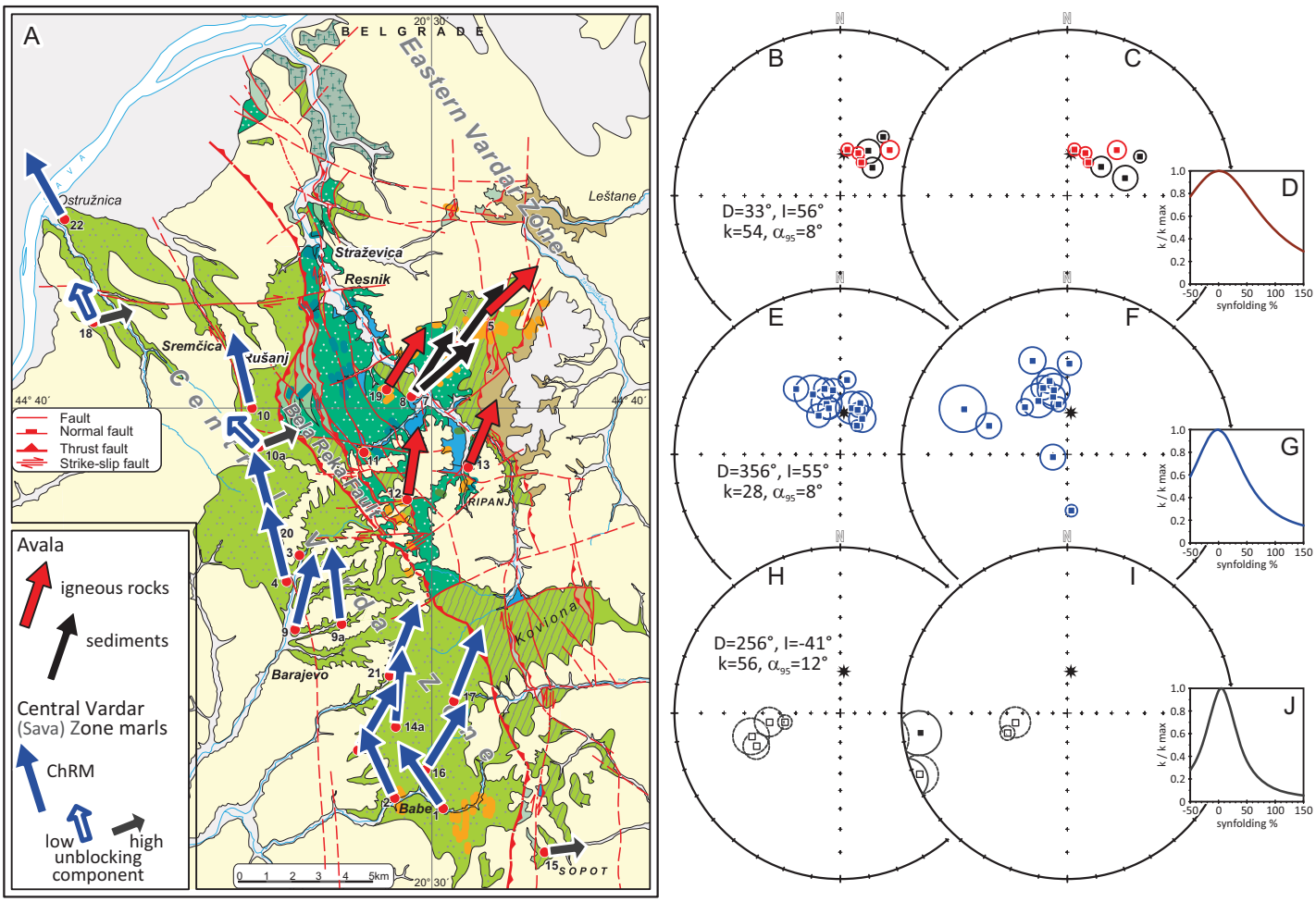

Fig. 6. Map of the locality mean declinations for the Belgrade area (A) and locality/site mean paleomagnetic directions before and after tilt corrections. For the Avala region (B-D: red symbols are for dykes, 3N and 1 R polarity, black ones for shallow water carbonates, all N polarity), for the Central Vardar Zone, all localities, except 18 and 10a (E-G, 12N and 1 R polarity) and for the enigmatic outliers among the Upper Cretaceous marls (H-J: localities 18, 10a, 15, in Fig. 6A, and a single one S of the Belgrade segment in Fig. 1). Stars represent the present day geomagnetic dipole field at the sampling area. Diagrams B, E and H are before, C, F and I after, tilt corrections. D, G, J are syn-tilting diagrams. The negative fold test for the Avala region only concerns the Upper Cretaceous platform carbonates, which were remagnetized during the Oligocene by the intrusions.

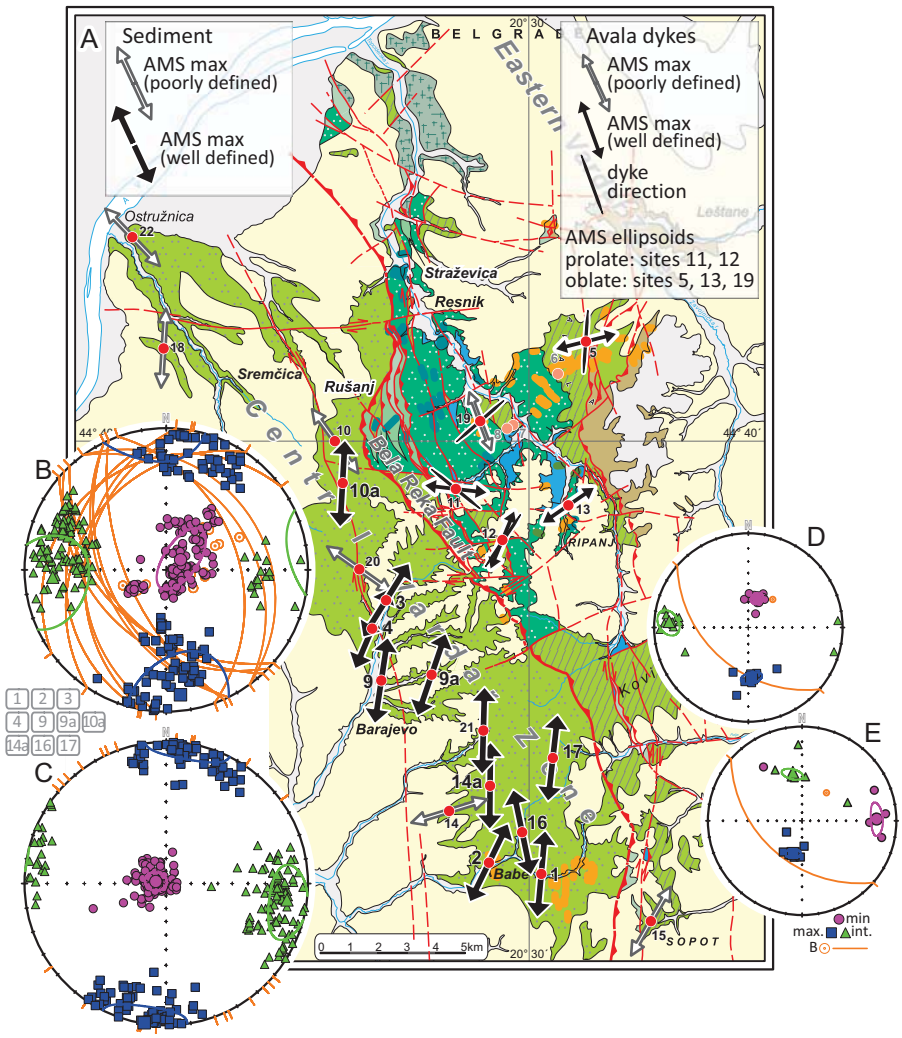

Fig. 7. Map of the AMS lineations (k1) for the dykes of Eastern Vardar Zone (Avala Mts) and for the flysch of the Central Vardar Zone, Belgrade area (A) and stereograms showing principal susceptibility directions which are well defined on locality level for the Upper Cretaceous marls of the Central Vardar Zone (B: before, C: after tilt correction). Comparison between the AMS (D) and AARM (E) fabrics for a typical marl outcrop (locality 1) shows the sub-parallel lineations of the bulk magnetic fabric and that of the magnetic minerals.

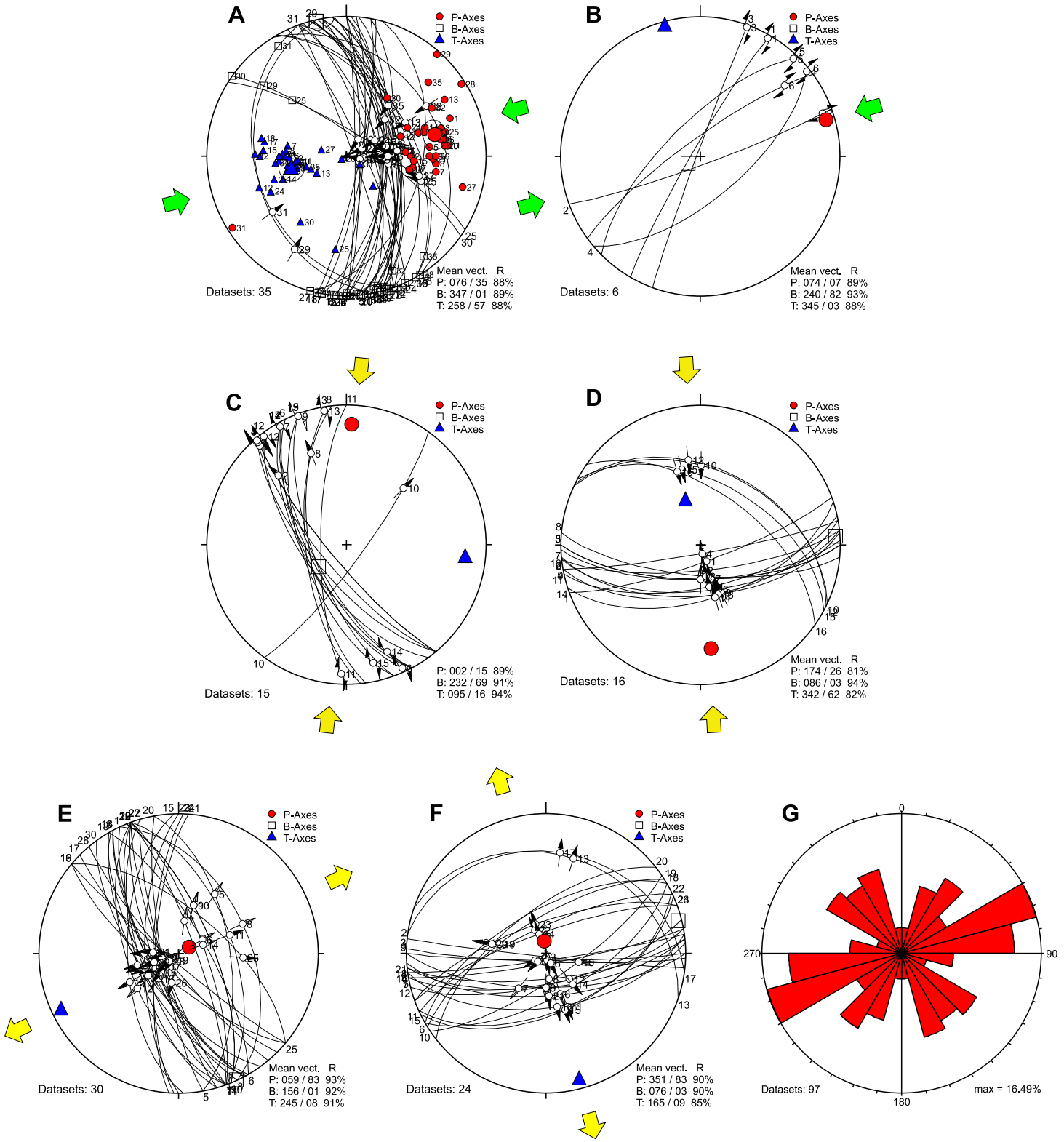

Fig. 8. Structural and kinematic data observed in the Belgrade area. Lines with arrows are stereoplots of faults with sense of shear, derived from kinematic indicators (such as slickensides or Riedel shears). A and B are kinematic data for the Late Cretaceous-Paleogene shortening events. C and D are kinematic data for the Early Oligocene shortening events. E and F are kinematic data for the Oligocene-Early Miocene phases of extension, G is a rose diagram of directions of Oligocene-Miocene dykes in vicinity of Belgrade.

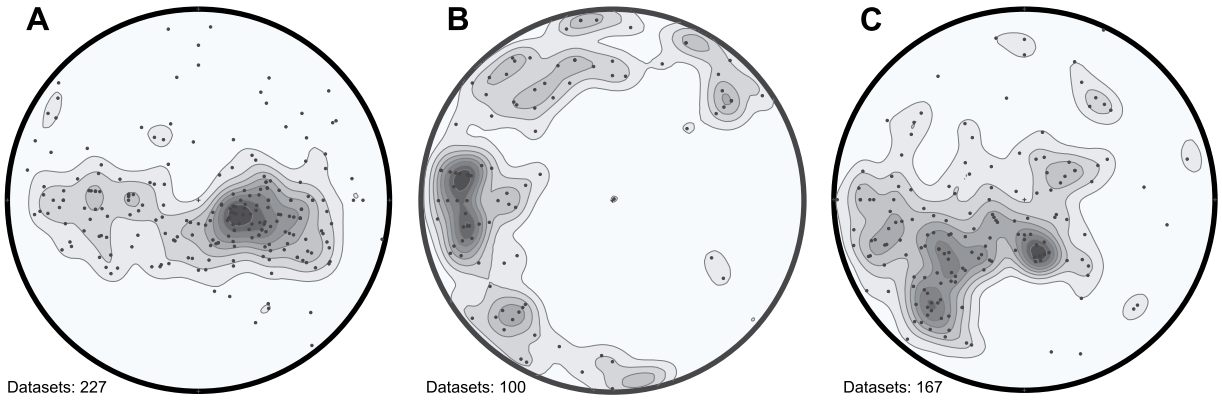

Fig. 9. Contour diagrams of the measured beddings planes of Upper Cretaceous deposits west of the Bela Reka Fault: south of Barajevo (A), between Barajevo and Sremčica (B) and the Ostružnica area (C). For the localities see Fig. 2.

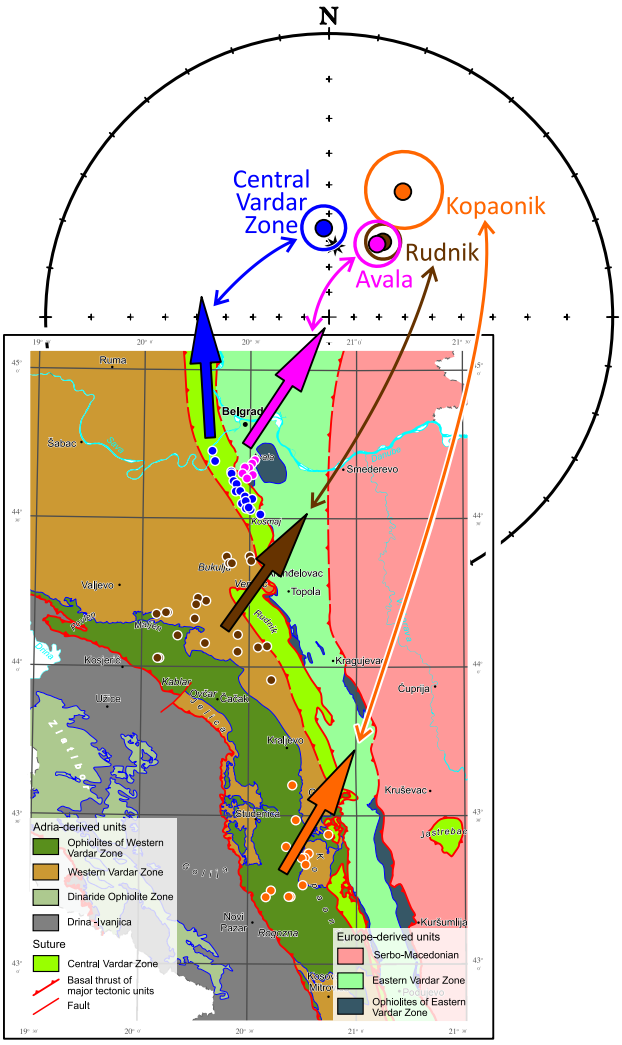

Fig. 10. Comparison of the overall-mean paleomagnetic directions with α95 from different segments of the Vardar Zone. The stereographic projection shows the overall-mean paleomagnetic directions for Oligocene magnetizations (Avala, Rudnik, Kopaonik) and for the 1st group localities from the Central Vardar (suture) Zone, where the magnetizations were probably imprinted around 40 Ma. Overall-mean declinations for the same areas are plotted on the geological map. Star represents the present day geomagnetic dipole field at the sampling area.

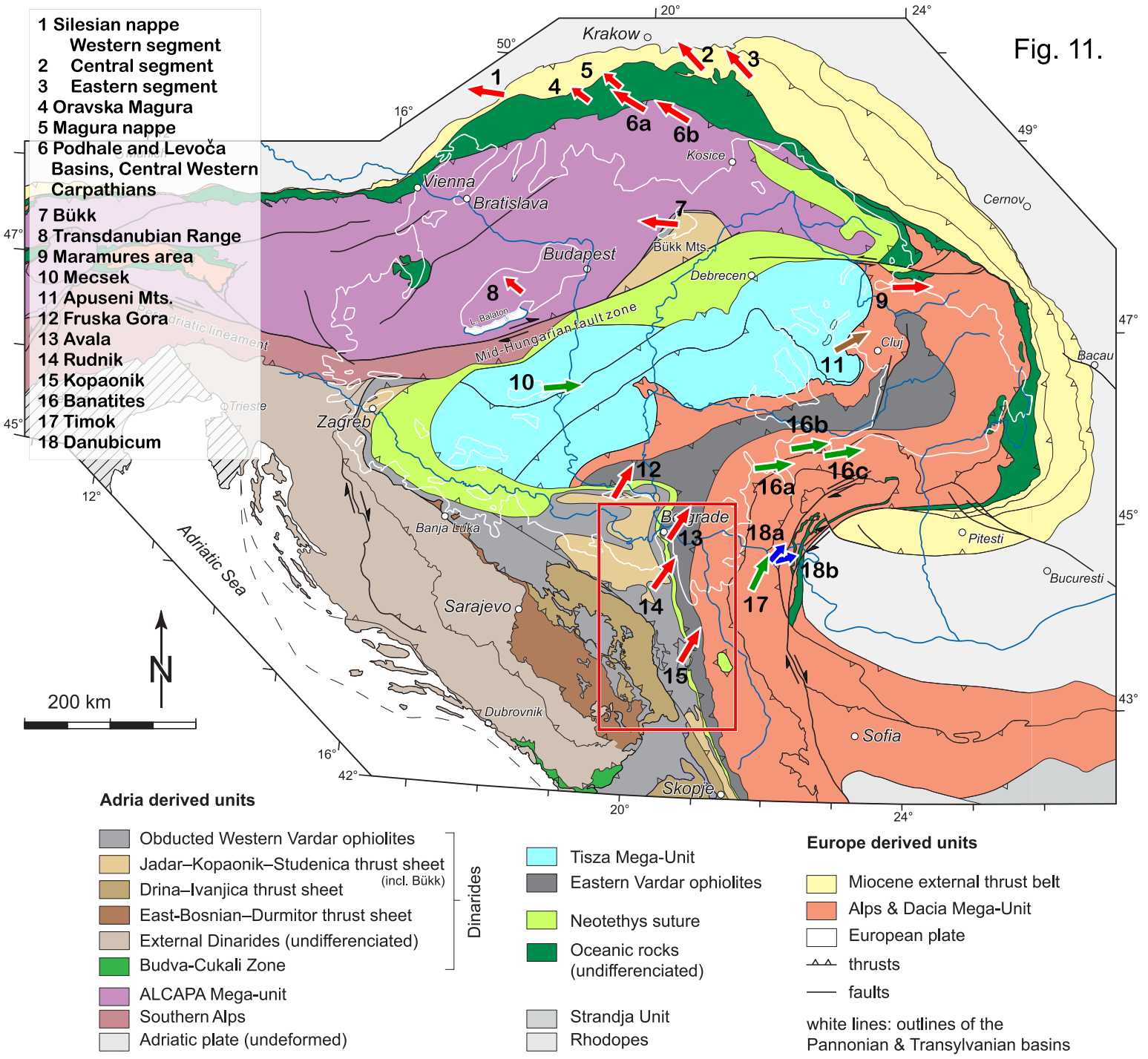

Fig. 11. Paleomagnetic evidence for vertical axis rotations in the Carpatho-Pannonian and North-Balkan region. Arrows represent overall-mean paleomagnetic declinations based on geographically distributed coeval localities from the following tectonic units: Silesian (1-3) and Magura (4, 5) nappes of the Outer Western Carpathians, Central Western Carpathians (6a and b), Salgótarján basin and B-kk Foreland (7), Transdanubian Range (8), Maramures area (9). Mecsek Mts (10), Apuseni Mts (11), Fruska Gora (12), Vardar Zone (13-15), Banatite belt (16a-c), Timok volcano-sedimentary complex(17), Danubicum (18a and b). Long arrows represent primary, short arrows post-deformational magnetizations. Colours are chosen according to the age of the source rocks: Red - Oligocene, Brown - Miocene, Green - Late Jurassic-Cretaceous. References: 1-3 and 6 Márton (2020), 4 Krs et al. (1991), 7 Márton and Márton (1996), 8 Márton and Fodor (2003), 9 Márton et al. (2007), 10 Balla et al. (2011), 11 and 16abc Panaiotu (1998), 12 Lesić et al. (2007), 13 present study, 14 and 15 Lesić et al. (2019), 17 Lesić et al. (2018), 18a Lesić et al. (2015), 18b Panaiotu (2012).

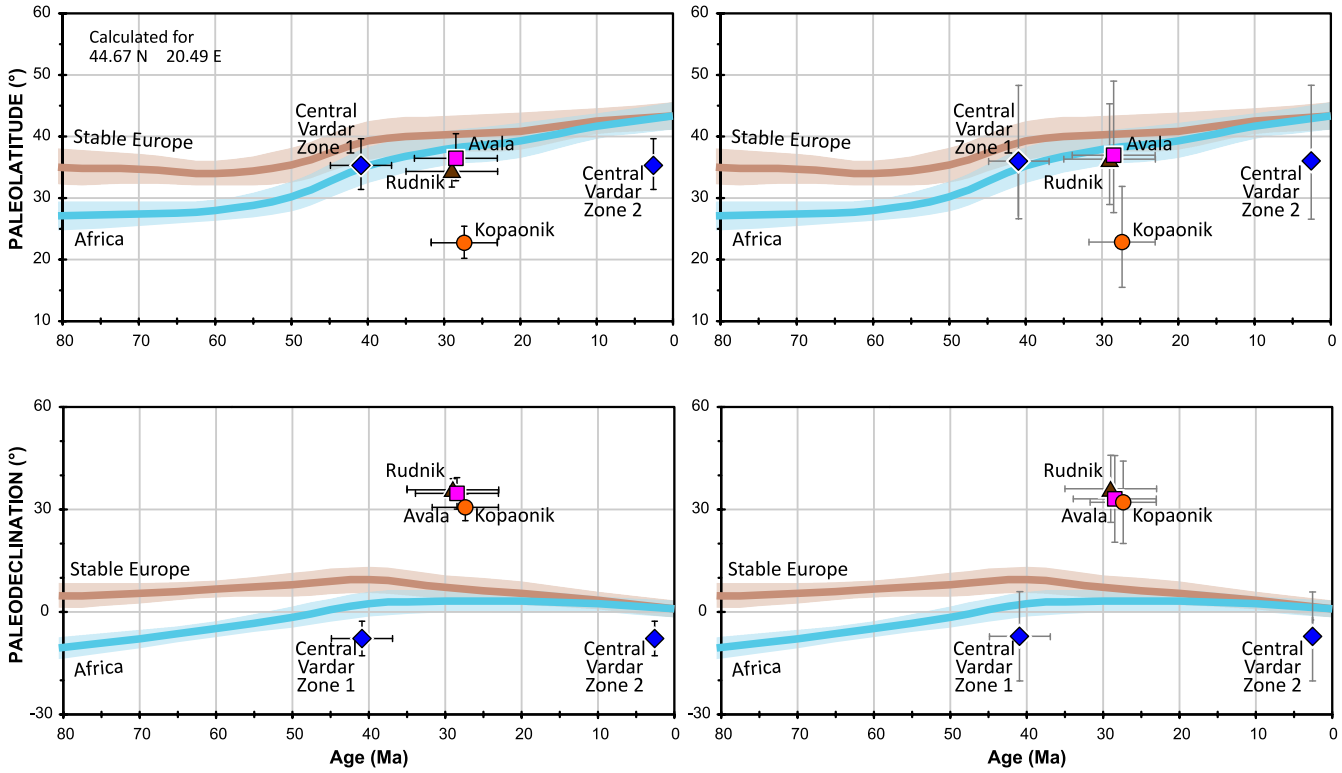

Fig. 12. Paleolatitudes and paleodeclinations for the Vardar Zone compared with those expected for stable Europe and Africa (Global APWP, Torsvik et al., 2012), respectively. For the Central Vardar (suture) Zone, where the magnetizations are of post-tilting/folding ages, two options are plotted. The one around 40 Ma is more likely (argued in chapter 5.1) and for perfect fit of paleolatitudes with those of the large plates. The error bars for the paleomagnetic results are based on number of samples (left side) and on localities/sites (right side). The error bars were computed based on Butler (1992). For apparent rotation and poleward displacement refer the Supplementary Table 1.

Fig. 13.

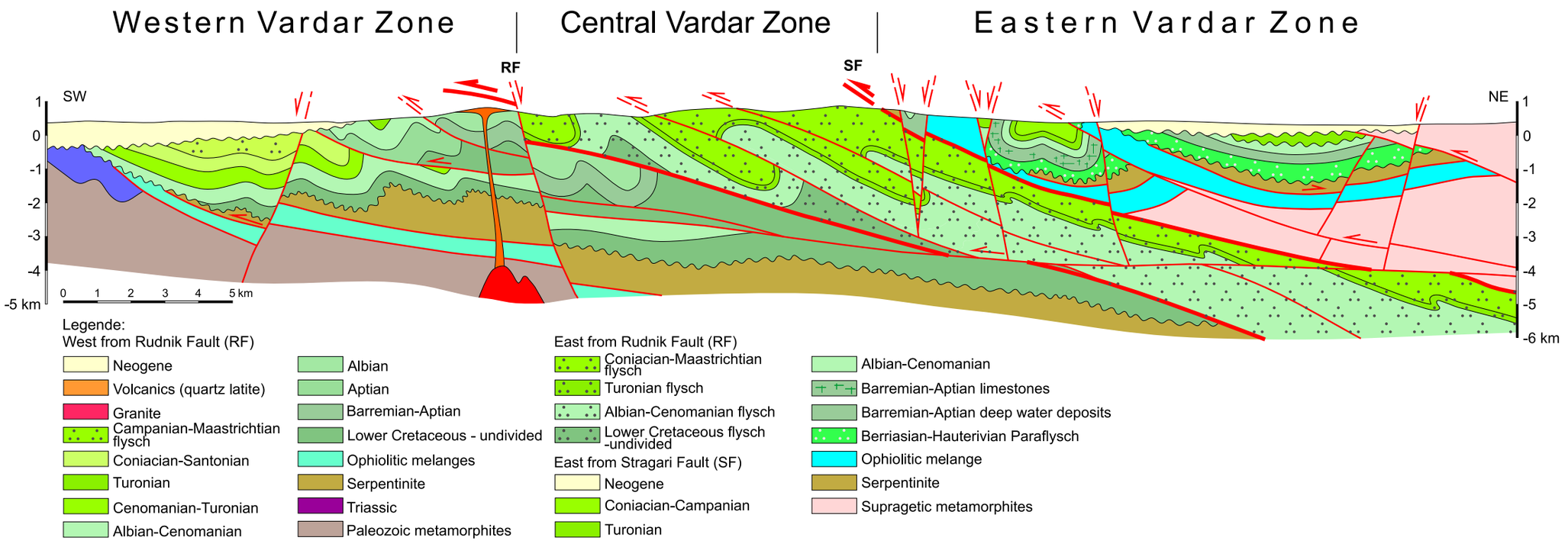

Fig. 13 Detailed cross-section from Rudnik to Topola area. The position of the cross-section is indicated in Figure 1 by the blue line. Note, cross-section is situated south of the Belgrade area. Major fault structures here are: Rudnik Fault (RF) - basal trust of Central Vardar Zone (Paleogene structure, Toljić et al., 2018), Stragari Fault (SF) basal trust of Eastern Vardar Zone - Cretaceous-Paleogene structure (southern prolongation of Bela Reka Fault, Toljić et al., 2018). Ophiolites of Eastern Vardar Zone and Western Vardar Zone were obducted in Late Jurassic (Schmid et al., 2008). The internal structures of all tectonic units are extremely complicated.

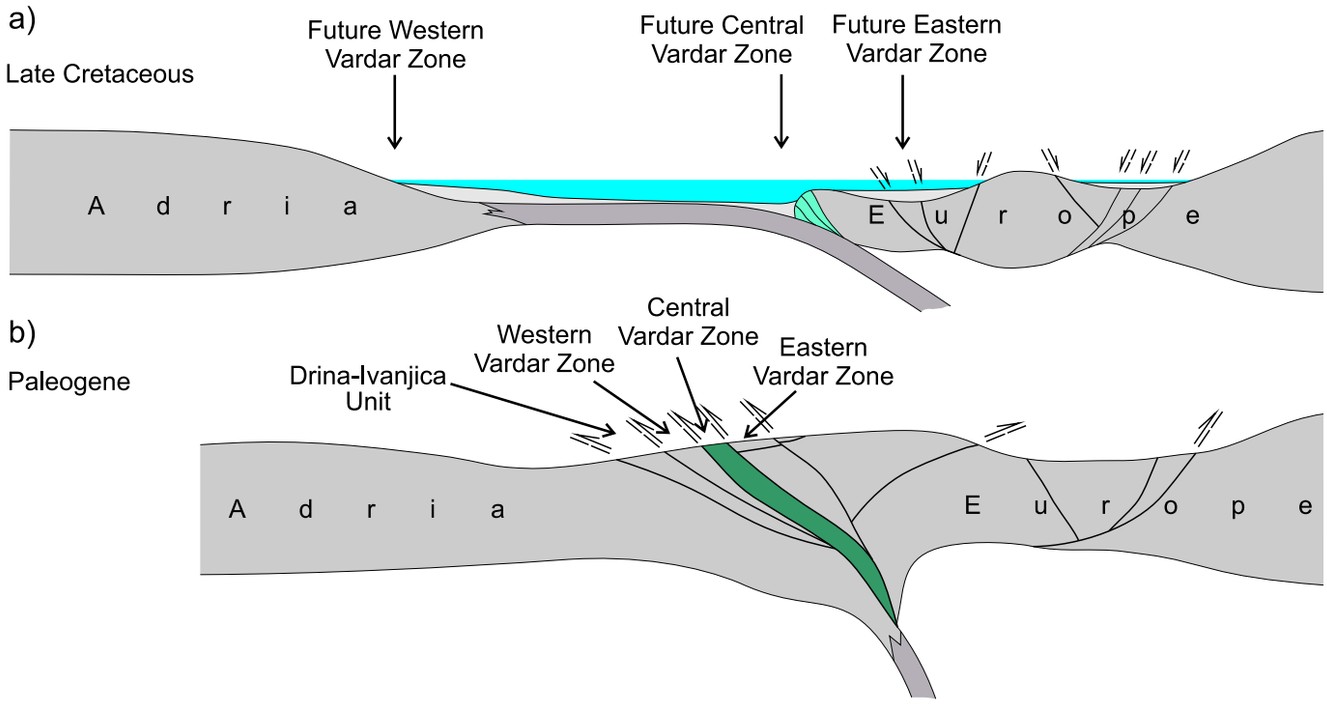

Fig. 14 Conceptual sketch of the evolution of the subduction-fore-arc-back-arc system during Cretaceous–Paleogene times in the Dinarides-Carpatho-Balkanides. a) Late Cretaceous times: low-angle subduction, b) Paleogene times: continental collision associated with contraction and thrusting (after Toljić et al., 2018).

Table 1

	Locality	age	lithology	Lat.N, Lon.E	alt.	n/no	D°	I°	k	α_{95}°	D_C°	I_C°	k	α_{95}°	dip	Lat.N.°	Lon.E.°	δp°	δm°
	East of Bela Reka fault																		
5	Avala 1 S 50-61	Oligocene	dyke + contact	44°41'50.2" 20°31'11.0"	381 m	10/12	47.3	+45.9	77.9	5.5					–	48.7	119.1	4.5	7.0
11	Bela Reka S 128-136	Oligocene	dyke	44°39'08.5" 20°27'45.1"	205 m	0/9				unstable					–				
12	Zovljak S 137-146	Oligocene	dyke	44°38'10.3" 20°29'01.3"	225 m	9/10	8.7	+58.6	142.0	4.0					–	81.6	146.9	4.7	6.4
13	Tešić majdan S 147-153	Oligocene	dyke	44°38'53.2" 20°30'38.7"	178 m	6/7	202.6	-58.9	329.0	4.0					–	72.6	119.3	4.7	6.3
19	Kurjakovac S 225-230	Oligocene	dyke	44°40'21.5" 20°28'29.1"	168 m	6/6	32.4	63.4	441.6	3.2					–	67.0	98.1	4.0	5.1
6	Avala 2, road up S 62-73	Coniacian-Maastrichtian	marly limestone	44°41'14.1" 20°30'32.2"	335 m	10/12	36.1	+42.7	198.1	3.4	61.7	+37.2	198.9	3.4	129/30	54.7	132.7	2.6	4.2
7	Avala 3, Kamenik S 74-88	Santonian	limestone	44°40'17.0" 20°29'31.0"	155 m	12/15	49.0	+61.2	91.4	4.6	49.5	+60.1	43.8	6.6	114/10 304/4	54.9	96.7	5.4	7.1
8	Avala 4, Beli Potok S 89-94	Santonian	limestone	44°40'15.4" 20°29'28.7"	154 m	5/6	32.5	+55.1	102.5	7.6	73.1	+50.1	102.5	7.6	134/30	63.6	119.0	7.7	10.8
15	Sopot S 166-174	Campanian	marly limestone	44°31'00.1" 20°32'56.4"	222 m	9/9	262.9	-43.5	36.9	8.5	262.3	+6.5	36.9	8.5	81/50				

West of Bela Reka fault

22	Ostružnica village S304-312	Coniacian-Maastrichtian	sandstone	44°43'43.0" 20°19'17.3"	85 m	5/9	330.8	+60.1	106.2	7.5	346.1	+50.7	106.2	7.5	27/14	68.4	290.7	8.6	11.4
18	Ostružnica S 205-210, 216-218	Early-Middle Maastrichtian	marl	44°41'43.0" 20°20'04.4"	124 m	8/9	255.4	-32.3	34.4	9.6	259.9	-54.8	34.4	9.6	346/23	22.5	107.5	6.1	10.8
						8/9	335.1	+55.8	14.1	15.3	338.7	+33.1	14.1	15		69.4	275.0	15.7	21.9
10	Sremčica* S 108-115	Coniacian-Maastrichtian	marl	44°39'37.1" 20°24'30.4"	199 m	7/8	346.5	+45.8	166.6	6.3	1.3	+32.7	166.6	6.3	48/22	69.5	236.7	5.1	8.0
10a	Sremčica Reka S 254-267	Coniacian-Maastrichtian	marl	44°39'12.3" 20°24'42.5"	197 m	14/14	248.6	-33.1	33.4	7.0	247.5	-2.2	18.8	9.4	54/24 70/36	27.7	111.9	4.5	7.9
						12/14	314.6	+36.0	10.5	14.1	340.1	+39.8	8.6	15.7		45.2	272.1	9.5	16.4
20	Krčevica S 231-241	Coniacian-Maastrichtian	marl	44°37'39.3" 20°25'15.3"	185 m	12/12	344.8	+55.0	23.3	9.7	348.1	+46.9	23.3	9.7	5/9	75.3	257.5	9.8	13.8
3	Barajevo 1 S 28-38	Coniacian-Maastrichtian	marly limestone	44°37'01.7" 20°26'02.5"	175 m	0/11				large scatter					324/15				
4	Barajevo 2 S 39-49	Coniacian-Maastrichtian	marl	44°37'02.3" 20°26'04.5"	169 m	10/11	346.1	+58.1	43.0	7.0	340.0	+43.9	43.0	7.0	324/15	78.1	265.8	7.6	10.3
9	Barajevo 3, Glumčevo brdo S 95-107	Coniacian-Maastrichtian	marl	44°35'34.9" 20°25'51.2"	158 m	11/13	14.0	+58.0	20.5	10.3	331.5	+49.8	20.5	10.3	277/31	78.0	135.1	11.2	15.2
9a	Jasenovac S 242-253	Coniacian-Maastrichtian	marl	44°35'41.5" 20°27'06.2"	188 m	11/12	353.5	+47.5	46.6	6.8	339.6	+28.0	46.6	6.8	304/26	73.2	220.6	5.7	8.8

21	Suva Reka, S 293-303	Coniacian-Maastrichtian	marly limestone	44°34'35.1" 20°28'30.2"	214 m	7/11	21.4	+53.3	70.5	7.2	346.4	+41.1	70.5	7.2	290/33	70.5	136.7	7.0	10.0
14	Lisović, Mišljevac S 154-165	Coniacian-Maastrichtian	marly limestone	44°33'09.1" 20°27'38.0"	309m	9/12	30.0	+67.4	198.5	3.7	175.9	+52.5	198.5	3.7	189/58 very tectonized	69.1	84.0	5.1	6.2
14a	Mišljevac S 268-278	Coniacian-Maastrichtian	marl	44°33'38.8" 20°28'40.3"	249 m	11/11	5.2	+41.5	82.0	5.1	318.0	+48.2	82.0	5.1	244/44	68.9	187.4	3.8	6.2
17	Parcanski vis S 191-200	Coniacian-Maastrichtian	marl	44°34'03.4" 20°30'28.9"	356m	8/10	21.3	+57.9	146.4	4.6	350.0	+56.0	146.4	4.6	282/20	73.0	123.8	5.0	6.8
16	Celevac, Pruten creek, S 183-187	Coniacian-Maastrichtian	marl	44°32'26.0" 20°29'27.1"	205m	5/5	31.6	+61.8	78.6	8.7	259.2	+79.9	78.6	8.7	224/36	67.3	103.2	10.4	13.5
1	Babe 3, S 1-17	Coniacian-Maastrichtian	marl	44°31'53.7" 20°30'01.7"	197m	9/10	145.9	-39.2	60.0	7.0	110.2	-36.7	60	7	221/43	54.2	263.1	5.0	8.4
2	Babe 2, S 18-27	Coniacian-Maastrichtian	marl	44°32'08.5" 20°28'44.7"	178m	5/10	335.5	+46.7	45.7	11.4	293.6	+21.7	46	11.4	246/59	64.4	258.4	9.5	14.7

Table 1. Summary of locality mean paleomagnetic directions based on the results of principal component analysis (Kirschvink 1980). Localities are numbered according to Fig. 2. Key: Lat.N, Lon.E: Geographic coordinates (WGS84) measured by GPS (Garmin GPSmap 60CSx), n/no: number of used/collected samples (the samples are independently oriented cores D, I (Dc, Ic): declination, inclination before (after) tilt correction; k and α_{95}: statistical parameters (Fisher 1953); Lat and Lon: coordinates of the paleomagnetic pole; δp and δm: half cones of the error ellipse of the paleomagnetic pole. *: intersection of remagnetization circles. Magnetic readings for the field orientation of the cores were corrected using IGRF-13 International Geomagnetic Reference Field model (Thébault et al. 2015).

Table 2

		N	D°	I°	k	α_{95}°	D_C°	I_C°	k	α_{95}°	Tests	Lat.	Long.	K	A95°
1	Central Vardar Zone Upper Cretaceous marls, ChRM	13	356.5	55.2	27.6	8.0	329.0	52.1	7.3	16.5	R-(i) γ 28.0 (c.γ 27.2) F- (0.6±25.0%)	81.7	213.7	16.6	10.5
2	Central Vardar Zone Upper Cretaceous marls, ChRM + 10a and 18 overprint components	15	351.4	54.6	22.9	8.2	331.0	49.8	8.0	14.3	Ro(i) γ 24.6 (c.γ 31.4) F- (11.5±27.2%)	79.8	235.2	14.2	10.5
3	Eastern Vardar Zone Oligocene magmatites and remagnetized Cretaceous carbonates	7	33.4	55.8	54.2	8.3	44.9	55.3	25.7	12.1	Rb, γ 7.7 (c.γ 25.7) F- (3.3±73.3%)	64.0	116.1	36.6	10.1
4	Western Vardar Zone Wider Rudnik area Oligocene – Miocene magmatites and remagnetized Cretaceous sediments	18	35.6	53.9	30.5	6.4	35.7	50.9	18.9	8.2	Rb. γ 7.1 (c.γ 12.8) F- (-17.8±54.2%)	61.6	114.8	20.0	7.9
5	Western Vardar Zone Wider Kopaonik area Oligocene magmatites	13	30.6	36.8	14.4	11.3	30.6	36.8	14.4	11.3	Rc. γ 13.9 (c.γ 22.5)	55.9	139.6	14.8	11.1

Table 2. Overall mean paleomagnetic directions and overall mean paleomagnetic poles for Belgrade area, West and East of Bela Reka Fault, for the Wider Rudnik and Wider Kopaonik areas. Lat and Lon of the paleomagnetic poles with statistical parameters are calculated from sedimentary locality mean directions before tilt correction (1 and 2) combined with site mean paleomagnetid directions for magmatites (3 and 4) or magmatites only (5).
Key: N: number of geographically distributed localities/sites; D°, I° and D_C°, I_C°: declination, inclination before and after tilt correction; k, α_{95}° and K, A95° statistical parameters (Fisher, 1953) of the palaeomagnetic directions and palaeomagnetic poles, respectively; R a, b, c, o, - (i: isolated observation): classification of reversal test (McFadden and McElhinny, 1990), a-c: positive, o: indeterminate, -: negative; F-: negative direction-correction tilt test (Enkin, 2003a).

Table 3

	Locality	Lat.N Lon.E	n	κ 10^{-6} SI	max D° D_C°	max I° I_C°	max conf	inter D° D_C°	inter I° I_C°	inter conf	min D° D_C°	min I° I_C°	min conf	Mean L(%)	Mean F(%)	Mean P(%)
5	Avala 1 dyke	44°41'50.2"	5	188±	255.8	25.7	11.0/3.0	84.8	64	19.7/8.4	347.5	3.6	20.1/5.3	0.6	1.1	1.7
	S 0050-061	20°31'11.0"		55.5												
5a	Avala 1 contact	44°41'50.2"	5	414±	108.7	2.5	37.5/5.5	18.1	15.2	37.5/3.8	207.6	74.5	7.6/1.5	0.3	3.4	3.8
	S 0050-061	20°31'11.0"		68.3												
11	Bela Reka	44°39'08.5"	6	10900±	96.7	21.5	7.3/4.7	308	65.3	7.4/5.5	191.4	11.7	8.1/4.5	0.9	0.6	1.7
	S 128-136	20°27'45.1"		1360												
12	Zovljak	44°38'10.3"	10	17100±	202.4	64.1	13.4/5.5	84.7	12.7	53.8/11.4	349.4	22.1	53.7/7.5	2.2	0.3	2.5
	S 137-146	20°29'01.3"		3250												
13	Tešić majdan	44°38'53.2"	6	244±	235.6	46.5	5.4/4.0	75	41.9	8.5/3.4	336.1	9.8	7.6/4.0	0.9	2.2	3.2
	S 147-153	20°30'38.7"		11.4												
19	Kurjakovac	44°40'21.5"	6	2850±	339.6	10.9	48.2/4.0	78.1	37.5	48.3/3.5	236.1	50.4	5.0/3.3	0.1	0.7	0.8
	S 225-230	20°28'29.1"		121												
6	Avala 2, road up	44°41'14.1"	12	975±	160.5	21.3	24.9/4.9	67.1	8.4	25.0/12.5	316.7	66.9	13.3/3.8	1.1	5.6	6.7
	S 62-73	20°30'32.2"		654	338.2	4.8		247.7	6.1		105.9	82.9				
7	Avala 3, Kamenik	44°40'17.0"	15	45.4±	61.0	21.1	43.6/32.5	251.0	68.6	61.5/34.5	152.3	3.4	61.7/44.3	0.5	0.3	0.8
	S 74-88	20°29'31.0"		30.2	63.1	22.9	42.0/26.1	231.2	66.7	67.5/25.9	331.3	4.3	67.7/40.4			
8	Avala 4, Beli Potok S 89-94	44°40'15.4"	6	319±	233.1	71.4	11.6/3.5	125.6	5.8	28.7/10.8	33.7	17.6	28.6/5.2	0.07	0.03	0.1
		20°29'28.7"		35.3	170.2	57.8		304.8	23.9		44.3	20.3				
15	Sopot	44°31'00.1"	9	129±	22.7	30.7	38.8/6.2	141.4	39.1	38.8/1.8	267.3	35.8	6.4/2.0	0.3	5.1	5.4
	S 166-174	20°32'56.4"		6.88	213.9	1.0		123.8	6.4		313.2	83.5				

22	Ostružnica village	44°43'43.0"	9	83±	140.2	13.7	20.9/3.9	48.9	5.5	20.8/3.9	297.5	75.2	5.5/2.6	0.4	2.6	3.0
	S 304-312	20°19'17.3"		5.2	136.4	18.8		229	7.5		339.8	69.7				
18	Ostružnica	44°41'43.0"	9	317±	4.4	17.2	45.9/3.8	273.6	2.6	45.9/3.6	175.2	72.6	4.6/4.1	0.2	9.6	9.8
	S 205-210	20°20'04.4"		11.9	183.6	4.7		93.2	4.3		320.6	83.6				
	S 216-218															
10	Sremčica	44°39'37.1"	7	309±	323.1	3.7	26.5/3.6	54.8	23.8	26.5/2.5	226.7	65.9	3.9/2.4	0.5	6.9	7.4
	S 0108-115	20°24'30.4"		5.75	324.2	1.6		54.2	1.9		195	87.5				
10a	Sremčica Reka	44°39'12.3"	14	202±	358.8	15	7.1/2.1	95.4	23.3	7.3/3.8	238.8	61.8	4.4/1.9	0.8	5.6	6.4
	S 254-267	20°24'42.5"		8.9	363.2	1.1	8.4/2.6	273.2	3.4	9.0/3.4	111.7	86.4	5.0/2.8			
20	Krčevica	44°37'39.3"	11	310±	304.7	6.2	54.8/2.8	214	6.5	54.8/6.5	77.7	81.0	6.9/2.9	0.1	4.0	4.1
	S 231-241	20°25'15.3"		12.3	305.3	1.7		214.8	14.4		41.7	75.5				
3	Barajevo 1	44°37'01.7"	11	307±	33	7.6	5.9/2.6	301.5	11.6	3.5/2.4	155.5	76.1	6.3/1.9	1.4	6.5	8.0
	S 028-038	20°26'02.5"		17.0	31.9	2		121.9	2.3		260.6	86.9				
4	Barajevo 2	44°37'02.3"	10	270±	25.1	13.1	4.5/2.5	292.5	11.2	4.5/3.4	163.1	72.7	4.3/2.2	1.8	7.6	9.6
	S 039-049	20°26'04.5"		4.84	23	5.5		113.1	1.7		219.8	84.2				
9	Barajevo 3, Glumčevo brdo, S 95-107	44°35'34.9"	11	283±	186.3	4.1	8.7/6.0	278.4	26.3	10.8/6.8	88.1	63.3	9.6/6.3	1.7	6.5	8.3
		20°25'51.2"		38.8	188.6	4.1	8.8/6.5	98.3	4.2	10.6/7.1	322.8	84.1	9.6/7.0			
9a	Jasenovac	44°35'41.5"	12	328±	195.7	2.2	9.2/2.9	286.3	14.3	6.5/3.8	97.0	75.6	7.8/4.1	1.9	3.1	5.1
	S 242-253	20°27'06.2"		24.3	198.4	9.9		106.5	10.6		330.7	75.4				
21	Suva Reka,	44°34'35.07"	8	307±	359.4	2.8	5.3/2.5	90.1	13.4	4.3/3.1	257.0	76.3	5.8/2.6	3.1	4.0	7.2
	S 293-303	20°28'30.19"		8.22	181.6	10.7		81.5	42.8		282.5	45.3				
14	Lisović, Mišljevac	44°33'09.1"	11	304±	252.8	38	22.9/9.7	125.6	37.7	47.2/18.7	9.3	29.8	47.3/16.6	0.5	0.1	0.6
	S 154-165	20°27'38.0"		37.0	234.0	1.8		144.0	1.4		16.6	87.7				

14a	Mišljevac	44°33'38.8"	11	295±	172.2	20.5	7.2/2.7	272.7	26.6	5.3/3.2	50.0	55.7	5.7/3.3	2.6	9.0	11.8
	S 268-278	20°28'40.3"		15.6	180.5	2.3	7.7/2.7	90.0	13.1	6.0/3.1	280.4	76.7	5.9/3.5	2.5	9.0	11.7
17	Parcanski Vis	44°34'03.4"	10	262±	7.9	4.8	7.9/2.6	277.2	7.6	3.4/2.2	129.8	81.0	7.7/2.5	2.0	5.9	8.1
	S 191-200	20°30'28.9"		24.0	6.4	3.5		97.2	12.3		261.0	77.2				
16	Celevac, Pruten creek,	44°32'26.0"	12	293±	161.6	19.2	8.3/2.5	257.9	17.6	12.7/3.0	27.3	63.4	14.1/4.2	3.4	2.8	6.2
	S 183-187	20°29'27.1"		45.5	348.2	1.3	6.8/2.6	78.7	17.3	9.8/3.0	254.0	72.6	10.7/4.9	3.4	2.9	6.4
1	Babe 3	44°31'53.7"	13	321±	176.4	33.5	10.2/5.2	273.0	9.8	9.7/7.0	17.1	54.7	7.2/5.9	2.9	6.1	9.2
	S 0001-017	20°30'01.7"		26.5	5.2	0.1		95.2	16.8		274.9	73.2				
2	Babe 2	44°32'08.5"	9	346±	185.2	43.6	6.4/4.4	294.6	19.2	4.6/2.9	41.7	40.1	6.4/3.0	3.7	5.7	9.7
	S 0018-027	20°28'44.7"		40.3	206.7	3.0		115.5	21.4		304.4	68.3				

Table 3. Summary of locality mean Anisotropy of Magnetic Susceptibility directions.

Key: n: number of samples (the samples are independently oriented cores); K: mean susceptibility; D, I, conf: declination, inclination and the related confidence ellipse of the maximum, intermediate and minimum directions (upper row before, lower row after tilt correction); P, L and F: degree of anisotropy, lineation and foliation. The results were evaluated using Anisoft 4.2 and 5.1 (Chadima and Jelínek, 2008, Chadima et al. 2018) based on Jelínek (1978).

Supplementary Table 1

	Stable Europe				**Central Vardar Zone**				44.67°N, 20.49°E	
	N	Pole lat. °	Pole lon. °	A95°	N *n*	Pole lat. °	Pole lon. °	A95°	Poleward displacement°	Apparent rotation°
0 Ma	24	88.5	173.9	1.9					7.2±7.9 *8.0±3.4*	-8.1±9.7 *-8.7±4.2*
5 Ma	18	89.1	110.3	1.7					8.5±7.8 *9.4±3.3*	-8.4±9.7 *-9.0±4.1*
10 Ma	49	86.7	150.0	1.8	15 *130*	79.8 *78.9*	235.2 *235.4*	10.5 *4.11*	6.4±7.8 *7.2±3.3*	-10.6±9.7 *-11.2±4.1*
40 Ma	24	81.1	144.3	2.9					3.2±8.0 *4.0±3.8*	-16.7±9.9 *-17.3±4.6*
	Africa									
0 Ma	24	88.5	173.9	1.9					7.2±7.9 *8.0±3.4*	-8.1±9.7 *-8.7±4.2*
10 Ma	49	86.6	170.0	1.8	15 *130*	79.8 *78.9*	235.2 *235.4*	10.5 *4.1*	5.6±7.8 *6.4±3.3*	-9.5±9.7 *-10.1±4.1*
40 Ma	24	80.5	189.0	2.9					-0.8±8.0 *-0.1±3.8*	-9.5±9.9 *-10.1±4.5*

	Stable Europe				**Eastern Vardar Zone**				44.67°N, 20.49°E	
	N	Pole lat. °	Pole lon. °	A95°	N *n*	Pole lat. °	Pole lon. °	A95°	Poleward displacement°	Apparent rotation°
30 Ma	24	83.1	146.5	2.6	7 *58*	64.0 *62.6*	116.1 *115.8*	10.1 *3.7*	3.3±7.7 *3.9±3.3*	25.8±9.6 *27.4±4.1*
	Africa									
30 Ma	24	82.9	180.3	2.6	7 *58*	64.0 *62.6*	116.1 *115.8*	10.1 *3.7*	0.9±7.7 *1.5±3.3*	30.0±9.6 *31.6±4.0*

	Stable Europe				**Western Vardar Zone Wider Rudnik area**				44.67°N, 20.49°E	
	N	Pole lat. °	Pole lon. °	A95°	N *n*	Pole lat. °	Pole lon. °	A95°	Poleward displacement°	Apparent rotation°
30 Ma	24	83.1	146.5	2.6	18 *179*	61.6 *60.8*	114.8 *118.8*	7.9 *2.7*	3.9±6.1 *6.1±2.8*	28.8±7.6 *28.4±3.5*
	Africa									
30 Ma	24	82.9	180.3	2.6	18 *179*	61.6 *60.8*	114.8 *118.8*	7.9 *2.7*	1.5±6.1 *3.7±2.8*	33.0±7.6 *32.7±3.4*

	Stable Europe				**Western Vardar Zone Wider Kopaonik area**				44.67°N, 20.49°E	
	N	Pole lat. °	Pole lon. °	A95°	N *n*	Pole lat. °	Pole lon. °	A95°	Poleward displacement°	Apparent rotation°
30 Ma	24	83.1	146.5	2.6	13 *136*	55.9 *56.7*	139.6 *141.6*	11.1 *3.6*	17.5±8.4 *17.7±3.3*	24.8±9.2 *23.3±3.8*
	Africa									
30 Ma	24	82.9	180.3	2.6	13 *136*	55.9 *56.7*	139.6 *141.6*	11.1 *3.6*	15.1±8.4 *15.3±3.3*	29.0±9.2 *27.5±3.7*

Supplementary Table 1. Poleward displacement and apparent rotation suggested by the paleomagnetic poles 2-5 of Table 3 with respect to stable Europe and Africa, respectively for the approximate time of the acquisition of the magnetization. For the results from W of the Bela Reka fault (Cenrtal Vardar Zone) alternative solutions are calculated, as the magnetization is of post-folding age. Calculations are based on Debiche and Watson (1995), Enkin (2003b). All reference poles are from Global Apparent Polar Wander Path by Torsvik et al., 2012, with the exception of 5Ma pole of Stable Europe by Panaiotu et al., 2012. In the table, the calculations are based on number of localities (normal print) and on number of samples (italic), respectively.